

**Variation in platinum group mineral and base metal sulfide assemblages
in the Lower Group chromitites of the western Bushveld Complex,
South Africa**

Bachmann, K.; Osbahr, I.; Tolosana-Delgado, R.; Chetty, D.; Gutzmer, J.;

Originally published:

September 2018

The Canadian Mineralogist 56(2018)5, 723-743

DOI: <https://doi.org/10.3749/canmin.1700094>

Perma-Link to Publication Repository of HZDR:

<https://www.hzdr.de/publications/Publ-25594>

Release of the secondary publication
on the basis of the German Copyright Law § 38 Section 4.

1 **Variation in platinum group mineral and base metal sulfide assemblages in the Lower Group**
2 **chromitites of the western Bushveld Complex, South Africa**

3 Running Title: PGM and BMS in the LG chromitites, western Bushveld

4

5 Kai Bachmann^{1,2*}, Inga Osbahr^{1,3}, Raimon Tolosana-Delgado¹, Deshenthree Chetty⁴, Jens Gutzmer^{1,2}

6 ¹Helmholtz-Zentrum Dresden-Rossendorf, Helmholtz Institute Freiberg for Resource Technology,

7 Bautzner Landstraße 400, 01328 Dresden, Germany

8 ²Department of Mineralogy, TU Bergakademie Freiberg, Brennhausgasse 14, D-09596

9 Freiberg/Sachsen, Germany

10 ³Deutsche Rohstoffagentur (DERA) at the Bundesanstalt für Geowissenschaften und Rohstoffe,

11 Wilhelmstrasse 25-30, 13593 Berlin-Spandau, Germany

12 ⁴Mineralogy Division, Mintek, Malibongwe Drive, 2125 Randburg, South Africa

13 *Tel: +49 351 260 4426

14 Fax: +49 351 260 4440

15 k.bachmann@hzdr.de

16

17

18

19

20

21

22 **Abstract**

23 The Lower Group chromitites of the Bushveld Igneous Complex are mined for chromite as a primary
24 product. The recovery of platinum group elements and base metals (Ni, Cu) as by-products has the
25 potential to add value to the chromite resources. This study focuses on the LG-6 and LG-6A
26 chromitite seams at the Thaba mine located on the western limb of the Bushveld Complex. Platinum
27 group minerals and base-metal sulfides are studied by mineral liberation analysis and electron
28 microprobe analysis to define distinct assemblages and to evaluate the potential for beneficiation.
29 Based on the results two distinct major mineral assemblages are defined: The first assemblage is rich
30 in platinum group element-sulfides, along with variable proportions of malanite/cuprorhodsitite and
31 alloys of Fe and Sn. The associated base metal sulfides are dominated by chalcopyrite and
32 pentlandite, along with pyrite and subordinate millerite/violarite. Associated silicates are mainly
33 primary magmatic orthopyroxene and plagioclase. The second assemblage is rich in platinum group
34 element-sulfarsenides and -arsenides as well as -antimonides and -bismuthides, which are associated
35 with a base metal sulfide assemblage dominated by pentlandite and Co-rich pentlandite. The
36 assemblage is also marked by an abundance of alteration minerals, such as talc, serpentine and/or
37 carbonates, which are closely associated with the platinum group minerals. Statistical evaluation
38 reveals that these two mineral assemblages cannot be attributed to their derivation from different
39 chromitite seams, but document the effects of pervasive hydrothermal alteration. Alteration
40 evidently had similar effects on the different chromitite seams. The occurrence and distribution of
41 the two characteristic assemblages has important implications for beneficiation. Assemblages rich in
42 platinum group element-sulfides associated with base metal sulfides respond well to flotation,
43 different to alteration assemblages rich in arsenides, antimonides and bismuthides. The nature of the
44 gangue minerals will also impact platinum group mineral recovery as high phyllosilicate abundances,
45 such as that encountered in the alteration assemblage may cause problems during flotation and lead
46 to poor recoveries.

47 **Keywords:** SEM-based image analysis, ANOVA, Cluster Analysis, PGM, Thaba Mine, Bushveld
48 Complex, EPMA

49 **Introduction**

50 The Bushveld Igneous Complex in South Africa is the world's largest layered mafic-ultramafic
51 intrusion. The Rustenburg Layered Suite (RLS), comprising the most significant portion of the
52 Bushveld Complex, consists of 7.5 to 9 km thick mafic and ultramafic cumulate rocks, covering an
53 area of approximately 65,000 km². The RLS was emplaced approximately 2,056 Ma ago
54 (2,055.91±0.26; Zeh et al. 2015) and can be subdivided into the Marginal, Lower, Critical, Main, and
55 Upper Zones (Hall 1932, Figure 1A).

56 The RLS hosts 21 chromitite seams (*e.g.*, Fourie 1959; Naldrett et al. 2012; 16 are shown in
57 Figure 1B). According to their stratigraphic position these are subdivided into lower, middle and
58 upper group chromitites. The Lower Group (LG) and Middle Group (MG) chromitites are extensively
59 mined for chromite as a primary product (*e.g.*, the mines Doornbosch, Winterveld, Lannex,
60 Tweefontein and Dwarsrivier; DERA 2013). The uppermost of the chromitite seams (UG-2), in
61 contrast, is exploited for platinum-group elements (PGE) as the primary economic product as it
62 reaches PGE concentrations up to 10 ppm Σ [PGE+Au] (Von Gruenewaldt et al. 1986; Lee 1996;
63 Cawthorn 2011). Base metals and chromite are recovered from the UG-2 as by-products. Whilst all
64 other chromitite seams do also contain elevated PGE concentrations, these range only from 0.5 to
65 3 ppm (Wagner 1929; Von Gruenewaldt 1977; Von Gruenewaldt et al. 1986; Lee and Parry 1988;
66 Cawthorn 1999; Barnes and Maier 2002; Naldrett et al. 2009a; Naldrett et al. 2012). Additionally, the
67 chromitites display a progressive increase in PPGE (Pt+Pd+Rh) from the LG to the UG chromitites,
68 whereas the content of IPGE (Os+Ir+Ru) remains broadly constant or increases only slightly (Naldrett
69 and von Gruenewaldt 1989; Scoon and Teigler 1994; Naldrett et al. 2009b). This trend coincides with
70 decreasing Cr/Fe ratios of the chromitites and results in a focus of mining the MG and LG seams for
71 chromite (DERA 2013). The exploitation of PGE in the MG and LG seams is currently regarded as sub-
72 economic (Oberthür et al., 2016).

73 Published knowledge on the mineralogy and deportment of PGE and base metals in the LG
74 chromitite seams is scant (Teigler and Eales 1993; Scoon and Teigler 1994; Naldrett et al. 2009b,
75 2012; Junge et al. 2016; Oberthür et al. 2016) and beside the investigation of Maier and Barnes
76 (Maier and Barnes 1999, and references therein) at Union Section, only scarce information is
77 available in particular for the northern part of the western limb of the Bushveld Complex. The UG-2,
78 in contrast, has been investigated in great detail (*e.g.*, McLaren and De Villiers 1982; Gain 1985;
79 Hiemstra 1985, 1986; Maier and Barnes 2008; Cawthorn 2011; Junge et al. 2014, 2015; Osbahr et al.
80 2014). Junge et al (2016) and Oberthür et al. (2016) emphasized the similarity of PGM of the LG-6
81 with the UG-2 chromitite. However, with samples derived for these studies from reworked chromite
82 dumps, they may yield representative results but lack any geological context. Given the scarcity of
83 published data, it is not surprising that the mechanism of PGE enrichment in chromitite seams
84 remains a subject of debate. Controversial aspects include the sulfide-poor nature of the RLS (S
85 contents commonly < 100 ppm; Scoon and Teigler 1994), and the presence of discrete PGM
86 containing almost the entire budget of PGE (*e.g.*, Hiemstra 1986).

87 Studies on the beneficiation characteristics of PGM and base metal sulfides (BMS) in Bushveld
88 chromitite seams other than the UG-2 are very scant – as most published contributions focus on
89 those resources currently exploited (UG-2, Platreef and Merensky Reef) (*e.g.*, Penberthy et al. 2000;
90 Bulatovic 2003; Shackleton et al. 2007a,b; Brough et al. 2010; Becker et al. 2008; Chetty et al. 2009,
91 Voordouw et al. 2010, Bushell 2012, Smith et al. 2013, Becker et al. 2014). These studies confirm that
92 characteristics such as quantitative mineralogy, deportment, mineral association and grain sizes play
93 a major role in PGM beneficiation. The type of PGM species, their liberation and association are
94 particularly relevant for floatability (*e.g.*, Penberthy et al. 2000; Chetty et al 2009) as well as the
95 association of PGM with BMS (Xiao and Laplante, 2004). PGM association with gangue minerals
96 displays a separate set of challenges for flotation processes (*e.g.*, Chetty et al. 2009). Furthermore,
97 Penberthy et al. (2000) reported that the grain size of PGM also affects floatability, with very fine (*i.e.*
98 <3 µm) PGM considered as slow floaters.

99 Despite these constraints a possible recovery of base metals and PGE as by-product during
100 exploitation of chromite would certainly add value and increase resource efficiency of chromite
101 mining ventures. A successful example in this regard is Sylvania Platinum Ltd., reworking chromite
102 dumps of the LG-6 and MG-1/2 chromitites from the eastern and western Bushveld Complex and
103 producing saleable concentrates of both PGE and chromite (Junge et al. 2016; Oberthür et al. 2016).

104 This study focuses on the LG-6 and LG-6A chromitite seams located at the Thaba mine, a chromite
105 mine situated on the western limb of the Bushveld Complex (Figure 1A) that is operated by Cronimet
106 Chrome Mining SA (Pty) Ltd., a subsidiary of the Cronimet Mining Group. The proven reserves at
107 Thaba total 23.6 Mt of chromite ore at 43.6 wt% Cr₂O₃ resulting in ca. 10 Mt contained Cr₂O₃ (DERA
108 2013). Mining started in 2011 and the life of mine is estimated at 26 years (DERA 2013). The mine
109 exploits the LG-6/LG-6A as well as the MG-1 to MG-4A chromitite seams. Any PGE recovery needs to
110 follow, or be integrated with, the recovery of chromite as the primary product.

111 In the present study, samples were obtained from three drill core intersections of the LG-6 and LG-6A
112 chromitites at Thaba mine. The aims of the study are:

- 113 (i) to characterize the PGM and base metal sulfide and Fe-sulfide (BMS) assemblages by *in-*
114 *situ* analysis of polished thin section surfaces of LG-6/LG-6A chromitite using scanning
115 electron microscopy–energy dispersive X-ray spectrometry (SEM-EDS)-based image
116 analysis techniques, complemented by electron microprobe analysis (EPMA),
- 117 (ii) to provide data on the composition of major silicate minerals and chromite,
- 118 (iii) to relate observed systematic changes in mineralogy and mineral association to
119 geological processes,
- 120 (iv) to discuss the obtained data with respect to published work and to assess implications
121 for the beneficiation of the chromitite ores.

122 The results are used to constrain the nature, distribution and origin of PGM and BMS in the
123 chromitites of the RLS. Furthermore, our study provides important constraints for eventual
124 beneficiation, as we consider not only qualitative mineralogy and mineral assemblage, but also
125 quantify relevant attributes such as mineralogy, mineral grain sizes and mineral association for PGM
126 and BMS. The *in-situ* methodology approach used in this study is preferred compared to the more
127 widely employed method of studying grain mounts of PGM concentrates (*e.g.*, Junge et al. 2016;
128 Oberthür et al. 2016) as it eliminates limitations to produce statistically significant results, for
129 parameters such as mineral association, as shown elsewhere (*e.g.* Penberthy et al. 2000; Voordouw
130 et al. 2010; Viljoen et al. 2012; Smith et al. 2013).

131 **Analytical Methods**

132 Access to diamond drill core intersections of LG-6 and LG-6A chromitite seams at Thaba mine was
133 granted by Cronimet Mining Group. Drill cores were logged to document the lithological architecture
134 of each intersection. Quarter drill cores were sampled with the goal to sample “pristine ores” below
135 the extent of present-day weathering, *i.e.* to depth in excess of 50m below the present-day land
136 surface, across the mine lease area. This approach was successful as none of the studied samples
137 revealed any evidence of supergene oxidation of BMS. Six different drill core locations were selected
138 for this study (Table 1), three of them for sampling of LG-6 (EL28, ZK149, ZK144) and three for LG-6A
139 (EL32, ZK136, SC42). Deflections were considered wherever available. Samples from deflections are
140 always demarcated by adding a D to the drill hole location name (Table 1). Chemical assay data for
141 some of the selected drill cores were made available by Cronimet Mining Group. Available assay data
142 refer always to entire chromitite seams; no assay data were available for drill cores ZK144, EL32D,
143 and ZK136D.

144 The general sampling approach follows that of Voordouw et al. (2010). To investigate, if the LG-6 is
145 bottom- or top-loaded with respect to PGM and BMS, each drill core intersection was divided into
146 five distinct sectors: sector 1 covers the bottom 10%, sector 3 the mid 40% and sector 5 the top 10%

147 of the seam (sector 2 and 4 are each 20 %). Each sector was sampled randomly to prepare an
148 individual polished thin section for study.. A similar approach was applied to the sampling of the LG-
149 6A, but samples of sector 1 and 5 were set onto the contact between host rock and chromitite
150 wherever this was possible. This resulted in a higher overall silicate proportion in the modal
151 mineralogy than for the LG6 samples. Each section was cut vertical to stratigraphy.

152 *Mineral Liberation Analysis (MLA)*

153 Thirty polished thin sections of ca. 150 μm in thickness were prepared at the Helmholtz Institute
154 Freiberg for Resource Technology (HIF). Each of these sections was analyzed twice by MLA on two
155 polished surfaces well-separated by re-grinding and re-polishing. These two surfaces are referred to
156 as surface A and surface B; all data and detailed investigations on the reproducibility of the MLA
157 measurements can be found in the electronic supplementary material (Appendix A, B and C). The
158 sections were analyzed twice to increase the number of PGM and BMS grains identified and to
159 constrain intra-sample variation. Furthermore, two sample surfaces were analyzed as in-run
160 duplicates to check for internal consistency of data acquisition.

161 The MLA instrument used in this study is located at the HIF and comprises a scanning electron
162 microscope FEI Quanta 650F equipped with two Bruker Quantax X-Flash 5030 energy-dispersive X-ray
163 spectrometers and the MLA 3.1.4 software suite for automated data acquisition. Consistent
164 operating conditions were applied (Table 2). DataView (Fandrich et al. 2007) software was used for
165 further processing of the data. All samples were analyzed using the sparse phase liberation (SPL_Lt)
166 and the grain X-ray mapping (GXMAP) mode (Fandrich et al., 2007). Standard spectra were collected
167 for all relevant minerals. Selected grains of silicates, BMS and PGM were then analyzed by electron
168 microprobe (EPMA, see below). More detailed information about the functionality of a MLA and the
169 joint offline processing of EPMA and MLA data can be found in Gu (2003) and Bachmann et al.
170 (2017).

171 As shown by Voordouw et al. (2010), abundances of individual PGM, sulfides and silicates may differ
172 from each other by an order of magnitude; the proportions of individual minerals are thus described
173 within chemically similar groups rather than in absolute terms (*e.g.*, area%^{PGM} refers to the area% of
174 individual PGM among all PGM).

175 *Electron probe microanalysis (EPMA)*

176 Electron probe microanalysis was performed with a JEOL JXA 8530F at the HIF equipped with a field
177 emission electron gun and five wavelength dispersive spectrometers (WDS). Five different analyzer
178 crystals TAP, PETJ, PETL, PETH, and LIFH on five spectrometers were utilized to measure chemical
179 compositions of various base metal and iron sulfides (BMS) as well as PGM. Quantitative EPMA
180 analyses were also performed on major silicates and chromite. Detailed information about the
181 methodology and the entire data set is provided in the electronic supplementary (Appendix A and D).

182 The assignment of the analyzed elements to detector crystals and spectrometers as well as peak and
183 background positions, dwell times and the lower limit of detection during PGM and BMS analyses are
184 shown in Table 3. All quantitative analyses were performed with a focused beam at an accelerating
185 voltage of 12 kV/ 20 kV and a beam current of 100 nA/ 30 nA. Analyses were corrected according to
186 the measurement protocol of Osbahr et al. (2015), slightly modified by a time-resolved offline
187 overlap correction and a step-wise overlap correction of multiple interferences. EPMA results were
188 further used to generate mineral standard spectra with a known composition for MLA
189 measurements.

190 *Statistics*

191 Statistical data evaluation and comparison of properties across the data set was obtained via
192 ANalysis Of VAriance (ANOVA, *e.g.* Fahrmeir and Hammerle, 1984), which explains the variance of
193 several target (predicted) variables by the influence of certain explanatory factors. In our case the
194 modal mineralogy in respectively area%^{PGM}, area%^{BMS}, area%^{Gangue} (Gangue: alteration silicates,
195 silicates, carbonates) are predicted variables. Other minerals occurring in trace quantities, such as

196 monazite, zircon, etc, were not considered as they add no relevant information. Chromite was not
197 considered because the chromite content is strongly dependent on the sampling location, *i.e.*
198 massive chromitite, chromitite with silicate intercalations or chromitite – host rock contact.
199 Explanatory factors considered were: The section surface (A/B), the relative stratigraphic position
200 within a seam “intra seam” (top, top-middle, middle, bottom-middle and bottom), and either the
201 seam (LG-6 vs. LG-6A) or the borehole (EL28D-LG-6, ZK149-LG-6, ZK144-LG-6, EL32D-LG-6A, ZK136D-
202 LG-6A vs. SC42-LG-6A, “inter-core” effects). ANOVA allows to test in an organized manner, which of
203 these variables exert a significant, systematic control on the area% composition of the mineral
204 groups considered. This is achieved by F-tests targeting each explanatory variable, and checking the
205 null hypothesis that the residual variability of a model including that target variable is the same as a
206 model without it. If this would be the case, then the target variable would not reduce the uncertainty
207 about the explained composition, and should be discarded. In practical terms, for those variables for
208 which the F-test returned a significance level of $p < 0.05$, the null hypothesis is rejected, hence the
209 target variable is accepted as having a significant influence on the composition. Significance levels
210 considered are: 0-0.001 highly significant, 0.001-0.01 moderately significant, 0.01-0.05 significant,
211 0.05-1 not significant.

212 A cluster analysis for the mineral association of PGM and BMS was performed to support the
213 separation into distinct ore types suitable for further treatment in a mineral beneficiation process.
214 The R software environment (R Core Team 2016) with the additional packages “mclust” (Fraley and
215 Raftery 2002) and “compositions” (van den Boogaart et al. 2014) were used for data analysis. The
216 algorithm “mclust” requires a choice of the characteristics (orientation, size and shape) of the
217 covariance matrix which are allowed to vary between groups: the analysis was done in “VVV”-mode,
218 meaning that each cluster was allowed to have a totally different covariance matrix (Fraley et al.
219 2012). All modal mineralogy subcompositions were treated with the statistical framework of
220 compositional data analysis (Aitchison, 1986; Tolosana-Delgado, 2012), to avoid the effects of

221 spurious correlation occurring in such closed subcompositions (Chayes, 1960). To get rid of these
222 effects, the solution chosen here is to work with ratios or log-ratios between components.

223 **Results**

224 Results are presented in three sections. The first provides a brief description of the lithological
225 architecture and qualitative petrographic appearance of the LG-6 and LG-6A chromitite seams
226 sampled. The following section reports the results of EMP analysis, *e.g.* the mineral chemistry of
227 PGM and BMS. This data is complemented by analyses of silicates and chromite provided in the
228 electronic supplement (Appendix A). Finally, MLA results are evaluated in terms of modal mineralogy
229 (sub-compositions PGM/BMS/Gangue as defined above) and mineral association (PGM/BMS).

230 *Lithology and Mineralogy*

231 This section provides largely qualitative descriptions of the studied chromitite seams – and their
232 mineralogy. Quantitative mineralogical data is provided later in this contribution. The LG-6 and LG-6A
233 chromitite seams at Thaba mine are well developed as massive, single seams that are usually hosted
234 by pyroxenite. The LG-6 seam as the primary mining target averages 0.85 m in thickness, varying
235 between 0.34 m and 1.37 m; the Cr₂O₃ content averages 43.1 % and the Cr:Fe ratio is 1.58. The LG-6A
236 occurs stratigraphically approximately 6 m above the LG-6 seam and averages at 0.23 m in thickness,
237 containing on average 41.2 % Cr₂O₃ with a Cr:Fe ratio of 1.48. Locally, cm-thin chromitite stringers
238 (such as in sample EL028-LG-6) or pegmatoidal pyroxenite (ZK136-LG-6A and EL32D-LG-6A) occur in
239 the pyroxenite host rock. Footwall (0.2 m) and hanging wall (1 m) of EL32D-LG-6A consist of
240 serpentinite (altered pyroxenite) while some of the pyroxenite in intersection ZK149-LG-6 is also
241 strongly serpentinitized.

242 All chromitite samples selected for this study are best described as massive chromitites that are
243 comprised mostly of chromite, orthopyroxene and plagioclase. Thin intercalations of silicate rocks as
244 well as up to a few cm long silicate oikocrysts are locally common in these massive chromitites.

245 Chromite grains are subspherical in shape, with average diameters of < 0.5 mm (max. ~1 mm), and
246 smooth grain margins. Chromite grains may host inclusions of silicates, sulfides and Fe-Ti oxides.
247 Subvertical veinlets are common, containing variable amounts of mica, amphibole and minor
248 carbonates. Especially in sample EL32D-LG-6A, chromite grains appear fractured and are cemented
249 by a younger generation of chromite.

250 The silicate minerals have been subdivided into two assemblages. The first assemblage includes
251 silicates regarded as orthomagmatic in origin (called silicates group), the other assemblage includes
252 all (hydrous) silicates that are considered to have formed by post-magmatic hydrothermal alteration
253 (called alteration silicates group). The silicates group is dominated by pyroxene (more orthopyroxene
254 than clinopyroxene), followed by feldspar, and traces of olivine, while quartz is almost absent. Mica is
255 present in very minor abundances and is biotitic in composition. Feldspar compositions are
256 dominated by plagioclase, alkali feldspar occurs only in trace amounts. In intersections ZK149-LG-6
257 and EL32D-LG-6A, feldspar is entirely absent.

258 The alteration silicates group is dominated by amphibole, chlorite (mainly clinochlor) and talc, while
259 only minor serpentine is present. Carbonate minerals (mainly of dolomitic compositions) were also
260 identified as part of the hydrothermal alteration assemblage and occur only in very minor amounts.
261 A notable exception is the occurrence of dolomite in chromitite seam LG-6A of drill core EL32D.

262 PGM and BMS occur in all samples in trace amounts. PGM are observed as monomineralic grains,
263 which may show internal zonation, but also as aggregates of variable complexity (for representative
264 examples see Figures 2B-H). Equivalent circle diameters (ECDs, value of the diameter of a circle
265 having the same area as the measured grain/particle; *e.g.*, Fisher et al. 1987) of PGM grains/
266 aggregates typically range between <1 and 20 μm , ECDs of up to 35 μm are scant. Average ECDs are
267 consistently between 4 μm and 5 μm . PGM are often locked or attached to BMS but also occur
268 enclosed in or interstitial to chromite, silicates and alteration silicates. PGM enclosed within chromite
269 grains consist mainly – but not exclusively - of laurite (Figure 2G). Members of the laurite $[\text{RuS}_2]$ -

270 erlichmannite [OsS₂] series are also the main carriers of IPGE (iridium-subgroup; Ir, Ru, Os). Minerals
271 belonging to the cooperite-braggite-vysotskite [PtS – (Pt,Pd)S – PdS] series and members of the
272 thiospinel solid solution series malanite [CuPt₂S₄]-cuprorhodsites [CuRh₂S₄] are major carriers of the
273 PPGE (platinum subgroup; Pt, Pd, Rh). Sperrylite [PtAs₂], PGE-antimonides, -bismuthides and -
274 bismuthotellurides such as geversite [PtSb₂], and stibiopalladinite [Pd_{5+x}Sb_{2+x}] with minor sudburyite
275 [PdSb], insizwaite [PtBi₂], and traces of genkinite [(Pt,Pd)₄Sb₃] and moncheite [(Pt,Pd)(Te,Bi)₂] are of
276 lesser abundance as are PGE-alloys including rustenburgite [Pt₃Sn] and tetraferroplatinum [PtFe].
277 Traces of native platinum [Pt] were also identified. Sulfarsenides (platarsite [PtAsS], hollingworthite
278 [RhAsS] and irarsite [IrAsS]) with variable compositions contribute significantly to the overall PGE
279 budget in some samples.

280 BMS usually occur as aggregates up to 300 μm in diameter or as single grains (<100 μm), interstitial
281 to chromite or enclosed in silicates. Smaller (up to 100 μm) aggregates of BMS were found as
282 inclusions in chromite. Importantly, pyrrhotite is almost absent. In general, BMS are dominated by
283 pentlandite [(Ni,Fe)₉S₈], which in some cases contains minor concentrations of Co. Other important
284 Ni-sulfides are millerite [NiS] and violarite [Fe²⁺Ni₂³⁺S₄]. Violarite often rims and replaces pentlandite
285 (Figure 2A, D). Some examples of millerite and violarite do also contain minor amounts of Co.
286 Chalcopyrite and pyrite only occur in some samples in significant amounts – relative to the other
287 BMS. Galena, stibnite and sphalerite were detected only in negligible abundance – they are not
288 considered further.

289 *Geochemistry and Mineral Chemistry*

290 5PGE+Au (Pt,Pd,Rh,Ir,Ru,Au) contents are around 1 ppm for LG-6 samples and 1.5 ppm for the LG-6A,
291 with a Pt/Pd ratio around 2.2 and 4 and Pt/Ru ratios around 0.9 for intersections ZK144-LG-6 and
292 ZK149-LG-6, respectively. In general, the total sulfur content ranges between 100 – 200 ppm
293 (<250 ppm), except intersection ZK144-LG-6, which contains only around 70 ppm. Arsenic contents

294 are usually below the detection limit (<0.5 ppm), except in a few samples of ZK149-LG-6 (up to
295 9 ppm). Detailed data is provided with the electronic supplement (Appendix A and E).

296 Mineral chemistry data was obtained for all relevant rock-forming mineral groups, except chlorite
297 and mica. Pyroxenes, amphiboles, serpentine and talc, as well as chromite compositions are well
298 discriminated by their mineral chemistry. Two different types of pyroxenes were detected, an
299 orthopyroxene (hereafter referred to as enstatite with $Mg/(Mg+Fe^{2+})$ ratios ranging from 0.82-0.84)
300 and a clinopyroxene with augitic to diopsidic composition (hereafter referred to as diopside).
301 Amphiboles can be best described as magnesio-hornblende. Feldspars yield plagioclase compositions
302 (Median = An_{66}). In general, chromite displays $Mg/(Mg+Fe^{2+})$ cation ratios around 0.42 (sample
303 EL32D-LG-6A around 0.33), while $Cr/(Cr+Al)$ cation ratios plot at 0.73 (EL32D-LG-6A: ~ 0.64). Detailed
304 data and methodology are provided in the electronic supplement (Appendix A and D).

305 The composition of PGM and BMS is collated in Tables 4 and 5. Mineral chemistry data were used to
306 provide proper identification of PGM in MLA data sets – and to characterize BMS in greater detail.
307 Pentlandite displays rather variable compositions, especially regarding the concentration of Co. For
308 the purpose of this study we refer to pentlandite containing > 2 wt% Co as Co-rich pentlandite. Pyrite
309 analyses reveal Co and Ni contents up to 1.5 wt% and 3.5 wt%, respectively.

310 A notable number of pyrite, pentlandite, Co-rich pentlandite and violarite analyses as well as a few
311 chalcopyrite analyses yielded measureable PGE concentrations. Pyrite, pentlandite and Co-rich
312 pentlandite yield concentrations up to 2-3 wt% Rh, Pt, Ru and Ir, around 1 wt% Pd and up to 0.5 wt%
313 Os. Chalcopyrite was found to contain PGE contents below 1 wt% and violarite up to 0.4 wt% Rh and
314 0.2 wt% Pd, respectively. Despite the fact that several previous studies have suggested that BMS can
315 contain significant amounts of PGE (Osbahr et al. 2013; Osbahr et al. 2014; Junge et al. 2014), the
316 concentrations reported in this study are unusually high. We tentatively consider the PGE as being
317 localized as submicroscopic inclusions of discrete PGM in the BMS (see Figure 2H), occasionally hit by
318 spot analyses during the EPMA measurements.

319 *Quantitative Mineralogy and Microfabric Data*

320 Quantitative mineralogical and microfabric data were obtained by MLA analysis. In order to facilitate
321 comparison, the rock-forming minerals were grouped as follows (sorted by abundance): Chromite
322 (Al-rich spinel, various chromite compositions), silicates (ortho- and clinopyroxene, feldspar, olivine,
323 quartz, biotite), alteration silicates (amphiboles, chlorite, muscovite, serpentine, talc), carbonates
324 (calcite, dolomite), others (*e.g.*, apatite, barite, monazite, rutile, titanite, zircon). For PGM and BMS
325 compositional sub-groups were defined (Table 6). The relative abundance of these is expressed as
326 $\text{area}\%^{\text{PGM}}$ and $\text{area}\%^{\text{BMS}}$ – this was done to ease comparison between different samples. The same
327 was done for gangue mineral groups (alteration silicates, silicates, carbonates) – these are expressed
328 as $\text{area}\%^{\text{Gangue}}$.

329 The quantitative mineralogy of all sampled seams is given in Table 7. For this purpose, data obtained
330 for all five samples collected from each seam was combined. Data for PGM and BMS for every thin
331 section surface analyzed is provided in the electronic supplement (Appendix C). This investigation
332 uses relative abundances of different PGM subgroups for classification. As illustrated in Figure 3A,
333 minerals belonging to the (Ru,Ir,Os)₂S₂ subgroup are present in all samples, but comprise rather
334 different proportions of the total PGM population (LG-6: 17 up to 59 total $\text{area}\%^{\text{PGM}}$; LG-6A: 6 up to
335 64 total $\text{area}\%^{\text{PGM}}$). In samples EL28D-LG-6, ZK144-LG-6, ZK136D-LG-6A and SC42-LG-6A (Pt,Pd)S and
336 (Pt,Rh)₂CuS₄ are common PPGE carriers subordinate only to alloys containing Fe and Sn; the latter
337 range from 30 to 68 total $\text{area}\%^{\text{PGM}}$ in the LG-6 and from 33 to 65 total $\text{area}\%^{\text{PGM}}$ in the LG-6A seam.
338 (Pt,Rh)₂CuS₄ is the dominant PPGE carrier in ZK144-LG-6. In contrast, the PGM assemblage in samples
339 ZK149-LG-6 and EL32D-LG-6A is dominated by (PGE)As,AsS and (PGE)Sb,Bi, comprising 44 to 76 total
340 $\text{area}\%^{\text{PGM}}$ in ZK149-LG-6 and 53 to 85 total $\text{area}\%^{\text{PGM}}$ in EL32D-LG-6A.

341 The BMS mineralogy is dominated by Co-rich pentlandite, chalcopyrite, millerite, violarite and pyrite
342 as well as traces of pyrrhotite (Figure 3B). The sulfide proportions are highly variable. In samples
343 ZK149-LG-6 and EL32D-LG-6A Co-rich pentlandite represents the majority of the BMS, while

344 chalcopyrite, pyrite as well as minor millerite dominate sample ZK144. Samples EL28D, ZK136D and
345 SC42 contain variable proportions of Co-rich pentlandite, chalcopyrite, pyrite/ (pyrrhotite), violarite
346 and minor millerite.

347 Figure 3C displays the relative distribution of PGM and BMS of intersections of the LG-6 and LG-6A
348 seams. While ZK144-LG-6 has a rather low BMS content and an assemblage dominated by
349 chalcopyrite and minor millerite, both Co-rich pentlandite dominated intersections (ZK149-LG-6 and
350 EL32D-LG-6A) display a high sulfide content (resulting in a distinctly higher sulfur content, *i.e.* sample
351 ZK149-LG-6 compared to sample ZK144-LG-6). In contrast, the PGM contents are rather similar, with
352 somewhat lower abundances in EL28D-LG-6 and EL32D-LG-6A and distinctly higher PGM contents in
353 sample ZK144-LG-6.

354 **Statistical Assessment**

355 The application of statistical methods is needed to deal with the large number of samples and the
356 multivariate datasets. This leads to the differentiation of three substantially distinct PGM-BMS
357 assemblages:

- 358 (I) PGM-sulfides and alloys of Fe and Sn \pm PGM-Cu-sulfides occur together with a BMS
359 assemblage dominated by pentlandite + chalcopyrite + pyrite
- 360 (II) PGM-Cu-sulfides \pm PGM-sulfides \pm alloys of Fe and Sn; corresponding BMS are dominated
361 by chalcopyrite + pyrite + millerite \pm pentlandite
- 362 (III) PGM-sulfarsenides and PGM-arsenides occur together with PGM-antimonides and -
363 bismuthides and scant tellurides; corresponding BMS are strongly dominated by
364 pentlandite and Co-rich pentlandite \pm chalcopyrite \pm pyrite.

365 The following sections document the relative contribution of ANOVA and cluster analysis to this
366 result.

367

368 ANOVA

369 An ANOVA was performed – followed by standard F-tests – to investigate the variability of the
370 samples and to determine assemblages for classification according to the sub-compositions
371 $\text{area}\%^{\text{PGM}}$, $\text{area}\%^{\text{BMS}}$ and $\text{area}\%^{\text{Gangue}}$. Detailed results can be found in the electronic supplementary
372 material (Appendix A). Results suggest that the “nugget effect” (small scale variability) is negligible
373 for all sub-compositions. The variance between samples of a different stratigraphic position within a
374 sampled seam, *i.e.* if seams have systematically different mineral assemblages within their respective
375 confines, should be noted – but remains small. Furthermore, there are no systematic changes in
376 mineral abundances observed between the two chromitite seams LG-6 and LG-6A. Thus, the
377 variability between certain drill cores explains up to 80 % of the total variability – depending on the
378 selected sub-composition. A detailed investigation of the ANOVA model showed a strong negative
379 correlation of PGE -sulfarsenides and PGE-antimonides, -bismuthides vs. PGE –sulfides, -Cu-sulfides
380 and -alloys of Fe,Sn (for $\text{area}\%^{\text{PGM}}$), along with (Co-rich) pentlandite against the other four BMS
381 considered, namely chalcopyrite, millerite, pyrite and violarite (for $\text{area}\%^{\text{BMS}}$). Furthermore, a
382 negative correlation of PGE-Cu-sulfides vs. PGE –sulfides and –alloys of Fe,Sn along with chalcopyrite
383 and millerite against pyrite and violarite was observed. The $\text{area}\%^{\text{Gangue}}$ assemblages are best
384 classified by separating alteration silicates and silicates-rich from carbonate-rich drill cores, followed
385 by a separation of alteration silicates from silicate-rich cores. While carbonate-rich samples are
386 associated with PGM-BMS assemblage (III), silicate-rich samples dominate PGM-BMS assemblage (I).
387 Significant amounts of alteration silicates may occur in samples belonging to PGM-BMS assemblages
388 (II) and (III).

389 *Cluster analysis*

390 For a quantitative assessment of the variability of the mineral association a cluster analysis was
391 performed according to the sub-compositions of PGM (without IPGE sulfides) and BMS. The results
392 were linked to the mineral assemblages defined in the previous chapter (ANOVA). Detailed
393 information can be found in the electronic supplementary material (Appendix A). Despite the very low

394 total abundance of BMS (< 0.02 area% in all samples), PGM show a strong preferred association with
395 BMS; they also show a close association with alteration silicates, occurring both in interstitial
396 positions and as inclusion. PGM are only to a much lesser extent associated with silicates and
397 chromite. PGM occur predominantly interstitial to chromite (with minor inclusions cf. Figure 2G).
398 BMS show a very similar association to PGM.

399 **Discussion**

400 Appropriate statistical assessment of quantitative mineralogical data suggests the presence of three
401 distinct PGM-BMS mineral assemblages in the LG-6 and LG-6A chromitite seams at Thaba mine. The
402 LG-6 and LG-6A intersections show striking differences between different drill cores, resulting in
403 variable PGM, BMS, and gangue mineral assemblages. The (para)-genetic relevance of the
404 documented differences between these three assemblages is evaluated below. Finally, implications
405 for recovery of PGM and BMS are briefly discussed.

406 *General Aspects*

407 The LG-6/LG-6A chromitites at Thaba mine share numerous similarities to lateral equivalents at
408 other locations in the Bushveld Complex (e.g., Teigler and Eales 1993; Eales et al. 1993; Scoon and
409 Teigler 1994; Naldrett et al. 2009b, 2012). Such similarities include:

- 410 (1) chromitites are developed as single seams hosted by pyroxenite,
- 411 (2) Cr:Fe ratio is 1.58 for the LG-6 and 1.48 for the LG-6A, respectively,
- 412 (3) orthopyroxenes yield $\text{Mg}/(\text{Mg}+\text{Fe}^{2+})$ ratios ranging from 0.82-0.84,
- 413 (4) intercumulus feldspar compositions within pyroxenites in the Lower Critical Zone are those of
414 labradorite (Median = An_{66}),
- 415 (5) limited variation in chromite compositions,
- 416 (6) uniform PGE grades (5E + Au) around 1 ppm (LG-6) and 1.5 ppm (LG-6A),
- 417 (7) Pt/Ru ratios around 0.9, Pt/Pd ratios ranging from 2 to 4, and low S_{tot} ranging from 70 to
418 200 ppm.

419 We thus deem it likely that the observations made here can be transferred to other occurrences of
420 LG chromitites within the Bushveld Complex.

421 *Mineral assemblages*

422 Different to previous investigations the present study offers quantitative mineralogical and
423 microfabric data on *in-situ samples* (*i.e.* polished thin samples not modified by comminution or
424 mineral separation) for PGM and BMS in the LG-6/LG-6A chromitites of the Bushveld Complex. The
425 data provide unique insight into different PGM, BMS and rock-forming mineral assemblages and
426 associations.

427 PGM assemblages are dominated by various Pt-Pd-Rh sulfides (cooperite-braggite and malanite-
428 cuprorhodsite), laurite (the main carrier of the IPGE), sulfarsenides, sperrylite and Pt-Fe alloys; PGE-
429 tellurides and PGE-bismuthotellurides are largely absent. These observations are rather similar to
430 previous studies (*e.g.*, Junge et al 2016; Oberthür et al. 2016) carried out on mineral concentrates.

431 BMS occur only in very minor abundances. Pentlandite, Co-bearing pentlandite, chalcopyrite and
432 pyrite dominate, whilst millerite is much less common. The virtual absence of pyrrhotite is noted. The
433 BMS mineralogy is thus rather similar to that reported in previous studies for Bushveld chromitites
434 (*e.g.*, Junge et al 2016; Oberthür et al. 2016).

435 Yet, despite these broad similarities, LG-6 and LG-6A chromitite intersections at Thaba mine reveal
436 significant and systematic mineralogical variations that remained previously unnoticed. These
437 mineralogical variations are observed in both the LG-6 and LG-6A – and can thus not be used to
438 distinguish the two seams from one another. Rather, the differences need to be described as lateral
439 variations independent of stratigraphic position.

440

441

442 Three different PGM-BMS assemblages were recognized (Figure 4):

- 443 (I) PGM-sulfides and alloys of Fe and Sn \pm PGM-Cu-sulfides occur together with a BMS
444 assemblage dominated by pentlandite + chalcopyrite + pyrite
- 445 (II) PGM-Cu-sulfides \pm PGM-sulfides \pm alloys of Fe and Sn; corresponding BMS are dominated
446 by chalcopyrite + pyrite + millerite \pm pentlandite
- 447 (III) PGM-sulfarsenides and PGM-arsenides occur together with PGE-antimonides, -
448 bismuthides and scant -bismuthotellurides; corresponding BMS are strongly dominated
449 by pentlandite and Co-rich pentlandite \pm chalcopyrite \pm pyrite

450 All three of these PGM-BMS mineral assemblages are interpreted to be the product of postmagmatic
451 alteration, variably modifying an orthomagmatic assemblage.

452 Mineral assemblage (I) can be regarded as the most pristine assemblage, revealing a low alteration
453 silicate to orthomagmatic silicate ratio. A relatively high BMS concentration and a variable PGM and
454 BMS mineral association mark this assemblage. BMS display variable abundances of pentlandite,
455 chalcopyrite, pyrite and minor violarite. PGE carriers are PGE sulfides and PGE-Cu sulfides with
456 variable proportions of PGE alloys of Fe and Sn. This is especially evident in intersection SC42-LG-6A,
457 which contains significant amounts of violarite. While traces of millerite in EL28D-LG-6 and SC42-LG-
458 6A as well as significant amounts of PGE alloys of Fe and Sn are consistent with beginning
459 desulfidization, violarite is typically regarded as a product of late stage hydrothermal alteration of
460 mixtures of iron-nickel sulfides (Dunn and Howes 1996; Tenailleau et al. 2006). Based on a statistical
461 analysis a "typical" mineral association for PGM in assemblage (I) was defined. The dominating PGE-
462 sulfides and -alloys of Fe and Sn are strongly associated to BMS and show only moderate affinity to
463 silicates and alteration silicates (Figure 5).

464 Assemblage (II), best typified by sample ZK144-LG-6, is marked by the abundance of alteration
465 silicates, although the alteration silicate to silicate ratio remains moderate. The total BMS content in
466 assemblage (II) is rather low, as is the total sulfur content (\sim 70 ppm). The BMS assemblage is

467 dominated by chalcopyrite, pyrite and millerite. Minerals of the malanite-cuprorhodsite solution
468 series are by far the most important carriers for PPGE in this assemblage.

469 BMS and PGM present in assemblage (II) suggest an origin by removal of Fe and S by either late
470 magmatic fluids and/or by reaction of sulfide with chromite from an orthomagmatic assemblage (e.g.
471 Naldrett et al 2012 and references therein). The high amounts of Ni-rich sulfides are explained
472 through re-equilibration of Fe from magmatic sulfide liquid with chromite (Naldrett and Lehmann
473 1988).

474 The high abundance of hydrous silicates associated with assemblage (II) suggests that corrosive
475 action of hydrothermal fluids further modified the BMS assemblage. That these fluids may play a
476 major role to explain the loss of sulfides was shown, for example, for the UG-2 (Penberthy and
477 Merkle 1999; Li et al. 2004, Voordouw et al., 2010). High malanite-group PGM concentrations in
478 chromitite were recently documented by Oberthür et al. (2016). The latter authors proposed that
479 part of the orthomagmatic chalcopyrite experienced a similar fate as the re-equilibrated Fe-sulfides
480 and has reacted to some extent with cooperite/braggite to form malanite. Although the PGM
481 mineralogy displays some similarities with assemblage (I), such as a similar PGM spectrum, the
482 mineral association of these PGM is distinctly modified and strongly dominated by alteration
483 silicates, minor silicates and lack of association with BMS.

484 Mineral assemblage (III) is best represented by intersections ZK149-LG-6 and EL32D-LG-6A and can
485 be further linked to gangue mineral assemblages. According to the ANOVA results, the gangue
486 mineral assemblage is closely related to assemblage (II). However, assemblage (III) generally displays
487 a significantly higher ratio in alteration minerals to orthomagmatic silicates; in drill core ZK149-LG-6
488 this is due to an abundance of alteration silicates, whereas in drill core EL32D-LG-6A carbonates are
489 particularly widespread. Host rocks of these two intersections display strong serpentinization and
490 thus provide further evidence for pervasive hydrothermal alteration. Furthermore, chromite analyses
491 display somewhat higher $Mg/(Mg+Fe^{2+})$ and $Cr/(Cr+Al)$ cation ratios (in sample EL32D-LG-6A). A

492 model including alteration by As-bearing fluids is favored over crystallization directly from As-bearing
493 melt as proposed by, e.g., Gervilla et al. (1996). Reasons for this interpretation include: (1)
494 Investigated samples have very low As contents and contain no other arsenides, such as nickeline,
495 etc., which would be expected in As-bearing melts. (2) PGE (sulf-)-arsenide-rich drill core
496 intersections display other prominent alteration features, as described above. (3) PGE arsenide-rich
497 assemblages of secondary origin are widely reported for the Bushveld Complex (Peyerl 1982; Kinloch
498 1982, Voordouw et al 2010). These arguments also support a secondary origin for PGE-antimonides
499 and -bismuthides. The PGE-(sulf)-arsenides, -antimonides and -bismuthides occur closely associated
500 with alteration silicates, carbonates or are interstitial to chromite. They show only a moderate
501 affinity to BMS and are almost absent as inclusions in chromite (Figure 5). Beside the carbonate-
502 dominated samples, the statistical assessment yielded similar results for the PGM mineral association
503 in assemblage (III) and assemblage (II), due to the strong affinity to alteration silicates. Nevertheless,
504 the low PGM affinity to silicates but higher affinity interstitial to chromite and to BMS, mainly
505 pentlandite, points to different processes responsible for the modification of the original
506 orthomagmatic mineral assemblage.

507 Laurite-group minerals, as the main IPGE carrier, deserve specific mention. They behave very
508 different to other PGM, and show stable proportions over all drill core intersections. According to the
509 statistical analysis laurite-group minerals remain unaffected by alteration processes. The same is true
510 for pyrite and pyrrhotite. Even though these two Fe-sulfides were reliably separated from
511 assemblage (III) in the ANOVA model, a further preferential association to assemblages (I) or (II) was
512 not possible to elucidate. This might be caused by the variable appearance of pyrite, as mineral of
513 primary (cf. Figure 2C) or possibly secondary origin (cf. Figure 2A, D), for example by replacing
514 pyrrhotite or as a by-product of the violarite alteration of pentlandite.

515

516

517 *Implications for beneficiation*

518 Given the fact that PGM and BMS were investigated *in-situ* in this study, the following relevant
519 parameters may be extracted and quantified from the data set for the potential recovery of PGM and
520 BMS: 1. Mineral species; 2. Mineral association; 3. Grain size distribution and 4. Gangue mineralogy
521 (*e.g.* Penberthy et al. 2000; Chetty et al. 2009). All these parameters are known to have a significant
522 impact on PGM recovery by flotation (*e.g.* Becker et al. 2013; Ndlovu et al. 2014).

523 Table 8 summarizes all relevant parameters of the three noted assemblages for mineral
524 beneficiation; similarities and differences between these assemblages are highlighted. Studies on the
525 floatability of different PGM species in the UG-2 chromitite (*e.g.* Penberthy et al. 2000; Chetty et al.
526 2009) suggest a higher floatability of sulfide-rich PGM assemblages compared to sulfarsenide-rich
527 assemblages. Flotation performance is also influenced by BMS and gangue mineralogy, as well as the
528 textural relations between PGM and associated minerals.

529 Relatively high recoveries may thus be expected for the BMS-rich assemblage (I), since the PGM
530 assemblage is not only sulfide-rich, but typically intergrown with a BMS assemblage marked by an
531 abundance of fast-floating chalcopyrite (Penberthy et al. 2000; Smith et al. 2013). In contrast, the
532 BMS content of assemblage (II) is significantly lower and PGM show rather little association to the
533 contained BMS. Therefore, recoveries of PGM may be expected to be somewhat lower, despite the
534 presence of PGM sulfides and chalcopyrite. Assemblage (III) can be expected to yield even lower
535 recoveries. This is due to the dominance of slow-floating sulfarsenides and a close association of
536 PGM with alteration silicates, chromite and carbonates – minerals that either do not float
537 (chromite/carbonate) or that need to be depressed in the given flotation process (*e.g.*, talc). The high
538 content of phyllosilicates in the alteration silicate association of assemblage (III) may be expected to
539 have rheological impacts in flotation, leading to even lower recoveries, as discussed by *e.g.*, Becker et
540 al. (2013) and Ndlovu et al. (2014).

541 In addition to the mineralogy of the three assemblages, the grain sizes of PGM and BMS will play an
542 important role in defining recoveries during flotation. The average grain size of 4-5 μm ECD for the
543 PGM and up to 300 μm ECD for BMS in all samples studied – irrespective of the actual assemblage.
544 This suggests that PGM and BMS should be amenable to flotation, if fully liberated and not reduced
545 further in size during comminution. PGM and BMS particle sizes $<3 \mu\text{m}$ are generally considered to
546 have poor flotation characteristics (Chetty et al. 2009). Nevertheless, to achieve sufficient liberation
547 of the majority of the minute PGM grains will likely require fine milling – beyond the typical flotation
548 feed of 45 – 80 % passing 75 μm typically used. However, the effects of ultrafine milling on liberation
549 characteristics of PGM and BMS mineral grains and grain aggregates are beyond the purpose of this
550 contribution. If PGM are associated with BMS – either because of intergrowth or because of the
551 presence of minute inclusions of PGM – the grain sizes of PGM may in fact not be relevant for
552 flotation - but rather the aggregate sizes and liberation of the BMS. These aggregates are typically
553 larger than 30 μm , often up to a few 100 μm which will easily float and further improve PGE
554 recovery.

555 **Conclusion**

556 Based on a combination of mineralogical and micro-analytical data, complemented by a tailored
557 statistical assessment, our study delivers the first systematic evaluation of PGM and BMS
558 assemblages in the LG's of the Bushveld Complex. According to our assessment, no truly unaltered
559 orthomagmatic mineral assemblage is preserved at the site of study – the LG-6 and LG-6A chromite
560 seams exploited at Thaba mine of the northernmost part of the western limb of the Bushveld
561 Complex. Alteration is documented by changes to the PGM, BMS and gangue mineralogy, while
562 chromite remains almost unaffected. Alteration assemblages are similar in both of the two studied
563 LG seams. It was further demonstrated that lateral variation between different drill cores dominates
564 over vertical variation within seam as well as between the LG-6 and LG-6A seams.

565 A “typical” PGM spectrum for all Bushveld chromitites as proposed by *e.g.*, Junge et al. (2016) or
566 Oberthür et al. (2016) is not supported by the results of the present study. Even though all included
567 groups of the “typical” PGM were detected, different assemblages of different origin can be
568 distinguished. This study thus extends the assemblages well-documented for the UG-2 (Kinloch 1982;
569 Peyerl 1982; Penberthy and Merkle 1999; Voordouw et al. 2010) to the LG chromitites. Our results
570 may be thus of general applicability, not only for the Thaba mine but also wider parts of the
571 chromitites of the Bushveld Complex, taking the similarities between, *e.g.*, the general mineralogy,
572 mineral chemistry, geology, host rocks within the Bushveld into account.

573 **Acknowledgements**

574 This is a contribution of the German/South African R&D project AMREP—Applied Mineralogy for
575 Resource Efficiency of Platinum-Group Metals—funded by the German Ministry of Education and
576 Research (BMBF; grant number BMBF 033R119E). We thank the Cronimet Mining Group for
577 providing access to their core shed and drill core intersections from the Thaba mine and for the
578 contribution of additional analytical data as well as information on the local geology and
579 beneficiation. Andreas Bartzsch and Roland Würkert are thanked for sample preparation and Dr.
580 Joachim Krause with his help at the EPMA. The comments of Thomas Oberthür to a previous version
581 of this manuscript are gratefully acknowledged.

582 **References**

- 583 Aitchison, J (1986) *The Statistical Analysis of Compositional Data*. Monographs on Statistics and
584 Applied Probability. Chapman & Hall Ltd., London (UK). (Reprinted in 2003 with additional
585 material by The Blackburn Press).
- 586 Bachmann K, Frenzel M, Krause J, Gutzmer, J (2017). Advanced Identification and Quantification of
587 In-Bearing Minerals by Scanning Electron Microscope-Based Image Analysis. *Microscopy and*
588 *Microanalysis* 23(3):527-537. doi: 10.1017/S1431927617000460
- 589 Barnes S-J, Maier W (2002) Platinum-group element distributions in the Rustenburg Layered Suite of
590 the Bushveld Complex, South Africa. In: Cabri LJ (editor) *The geology, geochemistry,*
591 *mineralogy and mineral beneficiation of platinum-group elements*. Canadian Institute of Min
592 Metall Pet Spec 54:431–458
- 593 Becker M, Brough C, Reid D, Smith D, Bradshaw D (2008) Geometallurgical characterisation of the
594 Merensky Reef at Northam platinum mine—comparison of Normal, Pothole and Transitional
595 reef types. In *Ninth International Congress for Applied Mineralogy*, Australasian Institute for
596 Mining and Metallurgy:391–399
- 597 Becker M, Yorath G, Ndlovu B, Harris M, Deglon D, Franzidis J-P (2013) A rheological investigation of
598 the behavior of two Southern African platinum ores. *Minerals Engineering* 49:92–97
- 599 Becker M, Wiese J, Ramonotsi, M (2014) Investigation into the mineralogy and flotation performance
600 of oxidised PGM ore. *Minerals Engineering* 65: 24–32
- 601 Brough CP, Bradshaw DJ, Becker M (2010) A comparison of the flotation behaviour and the effect of
602 copper activation on three reef types from the Merensky reef at Northam. *Minerals*
603 *Engineering* 23(11):846–854

604 Bulatovic S (2003) Evaluation of alternative reagent schemes for the flotation of platinum group
605 minerals from various ores. *Minerals Engineering* 16(10):931–939

606 Bushell, C (2012) The PGM flotation predictor: Predicting PGM ore flotation performance using
607 results from automated mineralogy systems. *Minerals Engineering* 36:75–80

608 Cawthorn RG (1999) Platinum-group element mineralization in the Bushveld Complex—a critical
609 reassessment of geochemical models. *South African Journal of Geology* 102:268–281

610 Cawthorn RG (2011) Geological investigations of the PGE distribution in the Bushveld Merensky and
611 UG-2 chromite reefs. *Journal South African Institute of Mining and Metallurgy* 111:67–79

612 Chayes, F (1960) On correlation between variables of constant sum. *Journal of Geophysical Research*
613 65(12):4185–4193

614 Chetty D, Gryffenberg L, Lekgetho TB, Molebale IJ (2009) Automated SEM study of PGM distribution
615 across a UG-2 flotation concentrate bank: implications for understanding PGM floatability.
616 *Journal of the Southern African Institute of Mining and Metallurgy* 109(10):587–593

617 DERA (2013) Rohstoffwirtschaftlicher Steckbrief für Chrom/Chromit. Deutsche Rohstoffagentur in der
618 BGR (DERA), 7pp

619 Dunn JG, Howes VL (1996) The oxidation of violarite. *Thermochimica Acta*, 282:305–316

620 Eales HV, Teigler B, Maier WD (1993) Cryptic variations of minor elements Al, Cr, Ti and Mn in Lower
621 and Critical Zone orthopyroxenes of the western Bushveld complex. *Mineralogical Magazine*
622 57:257–264

623 Fahrmeir L, Hammerle A (1984) *Multivariate Statistische Verfahren*. Walter de Gruyter, Berlin:796p

624 Fandrich R, Gu Y, Burrows D, Moeller K (2007) Modern SEM-based mineral liberation analysis.
625 *International Journal of Mineral Processing* 84:310–320.

626 Fisher, NI, Lewis T, Embleton BJ (1987) Statistical analysis of spherical data. Cambridge university
627 press.

628 Fourie GP (1959) The chromite deposits in the Rustenburg area. South Africa Geological Survey
629 Bulletin 27:45

630 Fraley C, Raftery AE (2002) Model-based Clustering, Discriminant Analysis and Density Estimation
631 Journal of the American Statistical Association 97:611–631

632 Fraley C, Raftery AE, Murphy TB, Scrucca L (2012) mclust Version 4 for R: Normal Mixture Modeling
633 for Model-Based Clustering, Classification, and Density Estimation. Technical Report No. 597,
634 Department of Statistics, University of Washington

635 Gain SB (1985) The geologic setting of the platiniferous UG-2 chromitite layer on the farm
636 Maandagshoek, eastern Bushveld Complex. Economic Geology 80:925–943

637 Gervilla F, Leblanc M, Torres-Ruiz J, Hach-Ali PF (1996) Immiscibility between arsenide and sulfide
638 melts; a mechanism for concentration of noble metals. Canadian Mineralogist 34(3):485–502

639 Gu Y (2003) Automated scanning electron microscope based mineral liberation analysis. Journal of
640 Minerals and Materials Characterization and Engineering 2:33–41

641 Hall AL (1932) The Bushveld igneous complex of the central transvaal. The Government Printer,
642 Pretoria, 560 pp

643 Hiemstra SA (1985) The distribution of some platinum-group elements in the UG-2 chromitite layer of
644 the Bushveld Complex. Economic Geology 80:944–957

645 Hiemstra SA (1986) The distribution of chalcophile and platinum-group elements in the UG-2
646 chromitite layer of the Bushveld complex. Economic Geology 81:1080–1086

647 Junge M, Oberthür T, Melcher F (2014) Cryptic variation of chromite chemistry, platinum group-
648 element and -mineral distribution in the UG-2 chromitite—an example from the Karee Mine,
649 western Bushveld Complex, South Africa. *Economic Geology* 109:795–810

650 Junge M, Wirth R, Oberthür T, Melcher F, Schreiber A (2015) Mineralogical siting of platinum group
651 elements in pentlandite from the Bushveld Complex, South Africa. *Mineralium Deposita* 50:41–
652 54

653 Junge M, Oberthür T, Osbahr I, Gutter P (2016) Platinum-group elements and minerals in the lower
654 and middle group chromitites of the western Bushveld Complex, South Africa. *Mineralium*
655 *Deposita* 51(7):841-852

656 Kinloch ED (1982) Regional trends in the platinum-group mineralogy of the critical zone of the
657 Bushveld Complex, South Africa. *Economic Geology* 77:1328–1347

658 Lee CA (1996) A review of mineralization in the Bushveld complex and some other layered intrusions.
659 In: Cawthorn RG (ed) *Layered intrusions*. Elsevier, Amsterdam, 103–145

660 Lee CA, Parry SJ (1988) Platinum-group element geochemistry of the lower and middle group
661 chromitites of the eastern Bushveld Complex. *Economic Geology* 83:1127–1139

662 Li C, Ripley EM, Merino E, Maier W (2004) Replacement of base metal sulfides by actinolite, epidote,
663 calcite and magnetite in the UG-2 and Merensky Reef of the Bushveld Complex, South Africa.
664 *Economic Geology* 99:173–184

665 Maier WD, Barnes S-J (1999) Platinum-group elements in silicate rocks of the Lower, Critical, and
666 Main zones at Union Section, western Bushveld Complex. *Journal of Petrology* 40:1647–1671

667 Maier WD, Barnes S-J (2008) Platinum-group elements in the UG-1 and UG-2 chromitites, and the
668 Bastard reef, at Impala platinum mine, western Bushveld Complex. *South Africa: Evidence for*

669 late magmatic cumulate instability and reef constitution: South African Journal of Geology
670 111:159–176

671 McLaren CH, De Villiers JPR (1982) The platinum-group chemistry and mineralogy of the UG-2
672 chromitite layer of the Bushveld Complex. *Economic Geology* 77:1348–1366

673 Naldrett A, Lehmann J (1988) Spinel non-stoichiometry as the explanation for Ni-, Cu, and PGE-
674 enriched sulphides in chromitites. In: Prichard HM (ed) *Geo-platinum 87*, Elsevier Science Publ
675 Ltd, 93–103

676 Naldrett A, von Gruenewaldt G (1989) Association of platinum-group elements with chromitite in
677 layered intrusions and Ophiolite Complexes. *Economic Geology* 84:180–187

678 Naldrett AJ, Wilson A, Kinnaird J, Chunnett G. (2009a) PGE tenor and metal ratios within and below
679 the Merensky Reef, Bushveld Complex: implications for its genesis. *Journal of Petrology*,
680 50(4):625–659. doi: 10.1093/petrology/egp015

681 Naldrett AJ, Kinnaird J, Wilson A, Yudovskaya M, McQuade S, Chunnett G, Stanley C (2009b) Chromite
682 composition and PGE content of Bushveld chromitites: part 1—the lower and middle groups.
683 *Trans Inst Min Metall B* 118:131–161

684 Naldrett AJ, Wilson A, Kinnaird J, Yudovskaya M, Chunnett G (2012). The origin of chromites and
685 related PGE mineralization in the Bushveld Complex: new mineralogical and petrological
686 constraints. *Mineralium Deposita* 47:209–232

687 Ndlovu B, Forbes E, Farrokhpay S, Becker M, Bradshaw D, Deglon D (2014) A preliminary rheological
688 classification of phyllosilicate group minerals. *Minerals Engineering* 55:190-200

689 Oberthür T, Junge M, Rudashevsky N, de Meyer E, Gutter P (2016) Platinum-group minerals in the LG
690 and MG chromitites of the eastern Bushveld Complex, South Africa. *Mineralium Deposita*
691 51:71–87. doi:10.1007/s00126-015-0593-0

692 Osbahr, I., Klemd, R., Oberthür, T., Brätz, H., and Schouwstra, R., 2013, Platinum-group element
693 distribution in base-metal sulfides of the Merensky Reef from the eastern and western
694 Bushveld Complex, South Africa: *Mineralium Deposita* 48:211–232

695 Osbahr I, Oberthür T, Klemd R, Josties A (2014) Platinum-group element distribution in base metal
696 sulfides of the UG-2, Bushveld Complex, South Africa—a reconnaissance study. *Mineralium*
697 *Deposita* 49:655–665

698 Osbahr I, Krause J, Bachmann K, Gutzmer J (2015) Efficient and Accurate Identification of Platinum-
699 Group Minerals by a Combination of Mineral Liberation and Electron Probe Microanalysis with
700 a New Approach to the Offline Overlap Correction of Platinum-Group Element Concentrations.
701 *Microscopy and Microanalysis* 21(05):1080–1095. doi:10.1017/S1431927615000719

702 Penberthy CJ, Oosthuyzen EJ, Merkle RKW (2000) The recovery of platinum-group elements from the
703 UG-2 chromitite, Bushveld Complex—a mineralogical perspective. *Mineralogy and Petrology*
704 68(1-3): 213–222

705 Penberthy CJ, Merkle RKW (1999) Lateral variations in the platinumgroup element content and
706 mineralogy of the UG-2 chromitite layer, Bushveld Complex. *South African Journal of Geology*
707 102:240–250

708 Peyerl W (1982) The influence of the Driekop dunite pipe on the platinum-group element mineralogy
709 of the UG-2 chromitite in its vicinity. *Economic Geology* 77:1432–1438

710 R Core Team (2016) R: A language and environment for statistical computing. R Foundation for
711 Statistical Computing, Vienna, Austria. URL <https://www.R-project.org/>

712 Scoon RN, Teigler B (1994) Platinum-group element mineralization in the Critical zone of the Western
713 Bushveld Complex: I. Sulfide-poor chromitites below the UG-2. *Economic Geology* 89:1094–
714 1121

715 Shackleton NJ, Malysiak V, O'Connor CT (2007a) Surface characteristics and flotation behaviour of
716 platinum and palladium arsenides. *International Journal of Mineral Processing* 85(1): 25–40

717 Shackleton NJ, Malysiak V, O'Connor CT (2007b) Surface characteristics and flotation behaviour of
718 platinum and palladium tellurides. *Minerals Engineering* 20(13): 1232–1245

719 Smith AJB, Viljoen KS, Schouwstra R, Roberts J, Schalkwyk C, Gutzmer J (2013) Geological variations in
720 the Merensky Reef at Bafokeng Rasimone Platinum Mine and its influence on flotation
721 performance. *Minerals Engineering* 52: 155–168

722 Teigler B, Eales HV (1993) Correlation between chromite composition and PGE mineralization in the
723 critical zone of the western Bushveld Complex. *Mineralium Deposita* 28:291–302

724 Tenailleau C, Pring A, Etschmann B, Brugger J, Grguric B, Putnis A (2006) Transformation of
725 pentlandite to violarite under mild hydrothermal conditions. *American Mineralogist* 91(4):
726 706–709

727 Tolosana-Delgado, R (2012) Uses and misuses of compositional data in sedimentology. *Sedimentary*
728 *Geology* 280: 60–79

729 Van den Boogaart KG, Tolosana R, Bren M (2014) compositions: Compositional Data Analysis. R
730 package version 1.40-1. <https://CRAN.R-project.org/package=compositions>

731 Viljoen F, Knoper M, Rajesh H, Rose D, Greeff T (2012) Application of a field emission mineral
732 liberation analyser to the in situ study of platinum-group element mineralisation in the
733 Merensky Reef of the Bushveld Complex, South Africa. In *Proceedings of the 10th International*
734 *Congress for Applied Mineralogy (ICAM)*, Springer, Berlin, Heidelberg: 757–764

735 Von Gruenewaldt G (1977) The mineral resources of the Bushveld Complex. *Minerals Science and*
736 *Engineering* 9(2):83–95

- 737 Von Gruenewaldt G, Hatton CJ, Merkle RKW, Gain SB (1986) Platinum-group element–chromite
738 associations in the Bushveld Complex. *Economic Geology* 81:1067–1079
- 739 Voordouw RJ, Gutzmer J, Beukes, NJ (2010) Zoning of platinum group mineral assemblages in the UG-
740 2 chromitite determined through in situ SEM-EDS-based image analysis. *Mineralium Deposita*
741 45:147–159. doi: 10.1007/s00126-009-0265-z
- 742 Wagner PA (1929) *The platinum deposits and mines of South Africa*. Oliver and Boyd, Edinburgh,
743 326pp
- 744 Xiao Z, Laplante AR (2004) Characterising and recovering the platinum group minerals—a review.
745 *Minerals Engineering* 17: 961–979
- 746 Zeh A, Ovtcharova M, Wilson AH, Schaltegger U (2015) The Bushveld Complex was emplaced and
747 cooled in less than one million years—results of zirconology, and geotectonic implications.
748 *Earth and Planetary Science Letters*, 418, 103-114
- 749

750 **Tables**

751 Table 1 General information and available bulk chemical data of all investigated samples.

Borehole	Length	From	To	Cr ₂ O ₃	FeO	SiO ₂	MgO	Al ₂ O ₃	CaO	P
<i>LG-6</i>	<i>in m</i>	<i>in m</i>	<i>in m</i>	<i>all data in wt%</i>						ppm
EL28	0.23	167.04	167.27	43.3	27.2	4.2	8.7	14.2	0.4	20
EL28D	0.30	167.45	167.75	43.5	28.1	3.1	8.5	16.3	0.4	20
ZK149	0.83	94.68	95.51	43.2	25.0	5.0	9.2	14.0	0.3	20
ZK149D	0.83	94.73	95.56	43.6	25.4	4.5	9.7	14.5	0.3	20
ZK144	0.87	294.98	295.85	-	-	-	-	-	-	-
ZK144D	0.93	294.89	295.82	44.0	26.9	3.5	8.7	13.6	0.3	20
<i>LG-6A</i>	<i>in m</i>	<i>in m</i>	<i>in m</i>	<i>all data in wt%</i>						ppm
EL32D	0.19	252.59	252.78	-	-	-	-	-	-	-
ZK136	0.20	268.95	269.15	44.7	25.7	4.1	11.3	14.6	0.4	28
ZK136D	0.20	269.22	269.42	-	-	-	-	-	-	-
SC42	0.25	344.60	344.85	43.8	23.2	4.1	9.7	14.2	0.2	25
SC42D	0.24	344.58	344.82	42.9	24.6	3.2	10.8	15.2	0.3	65

752 Please note that chromitite intersections in bold are considered in detail in this study. Boreholes
753 marked with "D" are deflections of the motherhole and regarded as their most similar sample.
754 Analyses were performed at Set Point Laboratories, Johannesburg. Cr₂O₃, FeO, SiO₂, MgO, Al₂O₃, CaO,
755 P were analyzed by X-ray fluorescence (XRF). "-" = no geochemical analyses are available.

756

757 Table 2 Summary of MLA parameters.

SPL parameters		GXMAP parameters	
Voltage (kV)	25	Voltage (kV)	25
Probe current (nA)	10	Probe current (nA)	10
HFW (μm)	750	HFW (μm)	1000
BSE calib.	Au 252	BSE calib.	Au 250
Resolution (pixels)	1000 × 1000	Resolution (pixels)	500 × 500
Pixel size (μm/px)	0.75	Pixel size (μm/px)	2
Quartz EDX-count	2000	Quartz EDX-count	2000
BSE Range	100 - 255	GXMAP trigger	25
Frame Guide Size (px)	30	Step size (px)	8 × 8
Min. grain size (px)	2	Min. grain size (px)	4

758 SPL = sparse phase liberation measurement mode, HFW = horizontal field width, BSE = back scattered
759 electrons, px = pixel, GXMAP = grain-based X-ray mapping measurement mode, EDX = energy
760 dispersive X-ray spectroscopy

761

762

763 Table 3 Instrumental parameters applied to PGM/BMS analysis on the EPMA.

Element/ Line	Spectrometer/ Crystal	Peak position (mm)	Lower Backgr. (mm)	Upper Backgr. (mm)	Measurement Time Peak (s)	Measurement Time Backgr. (s)	12 kV Limit of Quantification* Sulfide/ PGM (ppm)	20 kV Limit of Quantification* Sulfide/ PGM (ppm)	Standards (ASTIMEX Standards Ltd.)
As L α 1,2	1 TAP	105.14	6.127	6.563	60	15	213/ 297	330/ 480	Arsenopyrite_AST
S K α 1	2 PETJ	171.599	5.061	-	40	20	117/ 170	157/ 177	Pentlandite_AST
Pd L β 1	3 PETL	133.048	4.970	9.601	40	20	493/ 653	417/ 770	Palladium_AST
Rh L α 1,2	3 PETL	147.419	5.086	4.703	40	10	243/ 327	227/ 367	Rhodium_AST
Au M α 1	3 PETL	187.047	10.418	9.281	40	10	473/ 1023	603/ 817	Gold_AST
Pt M α 1	3 PETL	193.563	10.028	2.769	40	10	513/910	573/ 1050	Platinum_AST
Ir M α 1	3 PETL	200.458	4.410	3.024	40	10	536/970	597/ 1040	Iridium_AST
Os M α	3 PETL	207.728	4.093	3.127	40	10	543/ 880	597/ 940	Osmium_AST
Sb L β 1	4 PETH	103.058	8.361	9.804	40	10	467/ 763	450/ 620	Stibnite_AST
Te L α 1	4 PETH	105.095	10.989	7.960	40	10	210/ 330	197/ 270	Tellurium_AST
Ru L α 1	4 PETH	155.161	3.218	-	40	20	133/ 210	143/203	Ruthenium_AST
Bi M α 1	4 PETH	163.863	12.114	13.374	40	10	337/ 550	430/ 560	BismuthSelenide_AST
Mo L β 1	4 PETH	165.793	14.082	17.831	40	10	433/ 633	467/ 633	Molybdenum_AST
Cu K α 1	5 LIFH	107.259	1.960	2.131	40	10	867/ 1510	297/ 467	Copper_AST
Ni K α 1	5 LIFH	115.466	6.521	2.887	40	10	660/ 1130	257/ 427	Pentlandite_AST
Co K α 1	5 LIFH	124.555	3.106	2.745	40	10	473/ 787	240/ 343	Cobalt_AST
Fe K α 1	5 LIFH	134.797	5.100	3.000	40	10	383/ 633	197/ 313	Pentlandite_AST

764 All standards supplied by ASTIMEX Standards Ltd. Limit of Quantification = 10 × limit of detection.

765

Table 4 Representative EPMA analyses of major PGM. Z – numbers of atoms per formula unit. b.d.l. – below detection limit; apfu – atoms per formula unit.

No.	300	193	414	511	127	145	186	51	90	115	99	243	71	329	294	273	239	
Comment	EL28D-3_080	EL28D-2_071	ZK136D-2_054	ZK136D-2_113	SC42-2_097	SC42-2_115	SC42-2_156	SC42-2_021	ZK149-5_063	ZK149-5_088	ZK149-5_072c	EL32D-4_049	ZK149-5_044c	EL32D-4_135	EL32D-4_131	EL32D-4_079	EL32D-4_045	
Seam	LG-6	LG-6	LG-6A	LG-6A	LG-6A	LG-6A	LG-6A	LG-6A	LG-6	LG-6	LG-6	LG-6A	LG-6	LG-6A	LG-6A	LG-6A	LG-6A	
Mineral	Cooperite	Cooperite	Braggite	Vysotskite	Vysotskite	Vysotskite	Malanite	Laurite	Laurite	Laurite	Platarsite	Platarsite	Hollingworthite	Hollingworthite	Sperrylite	Geversite	Stibiopalladinite	
<i>all data in wt%</i>																		
As	bdl	bdl	bdl	bdl	bdl	bdl	bdl	bdl	bdl	bdl	27.64	29.08	35.02	30.14	35.11	0.6	bdl	
S	15.37	14.98	18.8	22.71	23.65	24.91	26.29	38.57	38	36.69	11.75	13.14	10.91	15.99	0.34	0.09	0.24	
Pd	0.43	0.59	26.46	32.71	46.6	63.25	0.1	bdl	bdl	0.06	bdl	0.03	bdl	bdl	3.26	bdl	66.9	
Rh	bdl	bdl	bdl	bdl	bdl	bdl	10.57	0.68	0.24	0.9	4.03	16.3	24.88	44.95	0.06	bdl	bdl	
Au	bdl	bdl	bdl	bdl	bdl	bdl	bdl	bdl	bdl	bdl	bdl	bdl	bdl	bdl	bdl	bdl	0.14	
Pt	80.27	80.18	53.24	34.9	16.49	0.38	38.77	bdl	bdl	bdl	35.45	22.07	24.06	0.36	48.59	42.33	0.06	
Ir	bdl	bdl	bdl	bdl	bdl	bdl	8.28	2.65	2.8	4.91	1.72	2.52	bdl	1.65	bdl	bdl	0.03	
Os	0.1	0.05	bdl	bdl	bdl	bdl	0.5	1.72	6.68	8.8	2.02	5.56	0.32	0.24	0.03	0.06	bdl	
Sb	bdl	bdl	bdl	bdl	bdl	bdl	bdl	bdl	bdl	bdl	bdl	0.43	bdl	3.77	4.45	47.52	30.42	
Te	bdl	bdl	bdl	bdl	bdl	bdl	bdl	bdl	bdl	bdl	bdl	bdl	bdl	bdl	0.02	0.25	bdl	
Ru	bdl	bdl	bdl	bdl	bdl	bdl	0.07	55.3	52.55	47.42	14.89	8.28	3.24	2.35	bdl	0.01	bdl	
Bi	bdl	bdl	bdl	bdl	bdl	bdl	bdl	bdl	bdl	bdl	bdl	bdl	bdl	bdl	5.12	7.96	bdl	
Mo	bdl	bdl	bdl	bdl	bdl	bdl	1.2	0.15	0.15	0.12	bdl	bdl	bdl	bdl	bdl	bdl	bdl	
Cu	0.04	0.04	0.08	0.1	0.18	bdl	12.06	0.02	bdl	bdl	bdl	bdl	bdl	bdl	bdl	0.01	bdl	
Ni	2.39	1.77	2.46	10.55	11.01	10.81	0.4	0.07	0.03	0.14	0.14	0.4	0.21	0.1	0.19	0.04	0.27	
Co	0.03	0.02	bdl	0.02	bdl	bdl	1.48	bdl	bdl	bdl	bdl	0.07	0.02	0.02	0.06	bdl	0.05	
Fe	1.89	2.05	1.11	1.37	1.34	1.05	1.42	1.18	0.73	1.37	1.34	0.52	0.28	0.7	0.43	0.68	0.69	
Total	100.52	99.67	102.15	102.37	99.26	100.41	101.14	100.35	101.18	100.41	98.98	98.37	98.92	100.26	97.66	99.55	98.79	
<i>all data is given as apfu</i>																		
As	-	-	-	-	-	-	-	-	-	-	0.963	0.959	1.154	0.851	1.688	0.036	-	
S	0.987	0.982	1.002	1.011	1	0.986	4.018	2	2.006	1.993	0.956	1.012	0.84	1.055	0.038	0.012	0.058	
Pd	0.008	0.012	0.425	0.439	0.594	0.754	0.004	-	-	0.001	-	0.001	-	-	0.11	-	4.863	
Rh	-	-	-	-	-	-	0.503	0.011	0.004	0.015	0.102	0.391	0.597	0.924	0.002	-	-	
Au	-	-	-	-	-	-	-	-	-	-	-	-	-	-	-	-	0.006	
Pt	0.847	0.864	0.466	0.255	0.115	0.002	0.974	-	-	-	0.474	0.279	0.304	0.004	0.897	0.969	0.002	
Ir	-	-	-	-	-	-	0.211	0.023	0.025	0.045	0.023	0.032	-	0.018	-	-	0.001	
Os	0.001	0.001	-	-	-	-	0.013	0.015	0.059	0.081	0.028	0.072	0.004	0.003	0.001	0.001	-	
Sb	-	-	-	-	-	-	-	-	-	-	-	0.009	-	0.066	0.132	1.743	1.933	
Te	-	-	-	-	-	-	-	-	-	-	-	-	-	-	0.001	0.009	-	
Ru	-	-	-	-	-	-	0.003	0.91	0.88	0.817	0.384	0.202	0.079	0.049	-	0.001	-	
Bi	-	-	-	-	-	-	-	-	-	-	-	-	-	-	0.088	0.17	-	
Mo	-	-	-	-	-	-	0.061	0.003	0.003	0.002	-	-	-	-	-	-	-	
Cu	0.001	0.001	0.002	0.002	0.004	-	0.93	0.001	-	-	-	-	-	-	-	0.001	-	
Ni	0.084	0.063	0.071	0.257	0.254	0.234	0.033	0.002	0.001	0.004	0.006	0.017	0.009	0.004	0.012	0.003	0.035	
Co	0.001	0.001	-	0.001	-	-	0.123	-	-	-	-	0.003	0.001	0.001	0.004	-	0.006	
Fe	0.07	0.077	0.034	0.035	0.033	0.024	0.125	0.035	0.022	0.043	0.063	0.023	0.012	0.027	0.028	0.055	0.095	
Z	2	2	2	2	2	2	7	3	3	3	3	3	3	3	3	3	3	7

Table 5 Representative compositions of major sulfide minerals (BMS) as analyzed by EPMA.

Mineral		S	Cu	Fe	Co	Ni	Pb
(1) Chalcopyrite	Median	34.62	32.91	30.28	bdl	0.02	bdl
	Range	33.77-37.19	31.71-33.27	29.63-32.05	bdl	bdl-0.20	bdl
(2) Pyrite	Median	53.32	0.02	45.01	0.61	0.33	bdl
	Range	49.21-55.17	bdl-0.37	41.34-46.52	bdl-1.49	0.01-3.46	bdl
(3) Pentlandite	Median	33.22	bdl	27.68	0.91	37.57	bdl
	Range	30.14-41.19	bdl-0.15	19.12-31.71	0.08-1.14	32.95-40.62	bdl
(4) Co-Pentlandite	Median	33.52	bdl	28.86	4.46	32.67	bdl
	Range	30.90-35.57	bdl	21.03-30.86	3.40-5.29	27.89-35.31	bdl
(5) Millerite	Median	35.73	bdl	2.56	bdl	61.39	bdl
	Range	35.13-37.78	bdl	2.17-4.59	bdl-0.80	57.86-62.18	bdl
(6) Violarite	Median	42.84	0.08	29.30	0.29	23.82	bdl
	Range	41-32-44.29	bdl-0.15	27.66-30.91	0.25-0.33	23.31-27.26	bdl

Notes: (1): n=43; (2): n=44; (3): n=70; (4): n=35, pentlandite analyses with >2.00 wt% Co; (5): n=3; (6): n=4; b.d.l. – below detection limit.

Table 6 Grouping of PGM (left) and BMS (right), respectively.

PGM			BMS		
Group	Mineral	Group _{Geostatistics}	Group	Mineral	Group _{Geostatistics}
(PGE)AsS	hollingworthite, irarsite, platarsite, sperrylite	PGM(1)	Ccp	chalcopyrite	BMS(1)
(Pt,Pd)S	cooperite, braggite, vysotskite	PGM(2)	Co-Pn	Co-rich pentlandite	BMS(2)
(Pt,Rh) ₂ CuS ₄	cuprorhodsite, malanite	PGM(3)	Mlr	millerite	BMS(3)
(Ru, Ir, Os)S ₂	erlichmannite, laurite	PGM(4)	Pn	pentlandite	BMS(4)
Alloys(Fe,Sn)	native platinum, rustenburgite, tetraferroplatinum	PGM(5)	Py/Po	pyrite, pyrrhotite	BMS(5)
Alloys(Sb,Bi)	geversite, insizwaite, stibiopalladinite, sudburyite	PGM(6)	Vio	violarite	BMS(6)

Table 7 Modal mineralogy of investigated LG-6 and LG-6A drill core intersections. All values are presented as area%.

Mineral	ZK144-LG-6	EL28D-LG-6	ZK149-LG-6	EL32D-LG-6A	ZK136D-LG-6A	SC42-LG-6A
Alteration Silicates	5.7	0.9	3.1	11.8	2.2	0.4
Carbonates	<0.1	<0.1	<0.1	3.7	<0.1	<0.1
Chromite	83.3	89.9	93.5	66.8	68.2	75.2
Silicates	10.8	9.2	3.4	17.7	29.6	24.4
Others	0.2	<0.1	<0.1	<0.1	<0.1	<0.1
Total	100.0	100.0	100.0	100.0	100.0	100.0

Table 8 Summary of important parameters of determined assemblages for mineral beneficiation.

Assemblage	PGM species	BMS species	Mineral association/ Gangue mineralogy		PGM grain sizes	BMS particle sizes
(I)	PGM-(Cu)-sulfides; alloys of Fe, Sn	Pn + Ccp + Py + Mlr	BMS, Chromite, Silicate		min: <1µm, max: 20µm, avg: 4-5µm	max: 300µm, avg: >30µm
(II)			alteration silicates	silicates		
(III)	PGM-(sulf)arsenides; alloy of Sb, Bi	(Co-rich) Pn ± Ccp ± Py		carbonates, chromite		

Figures

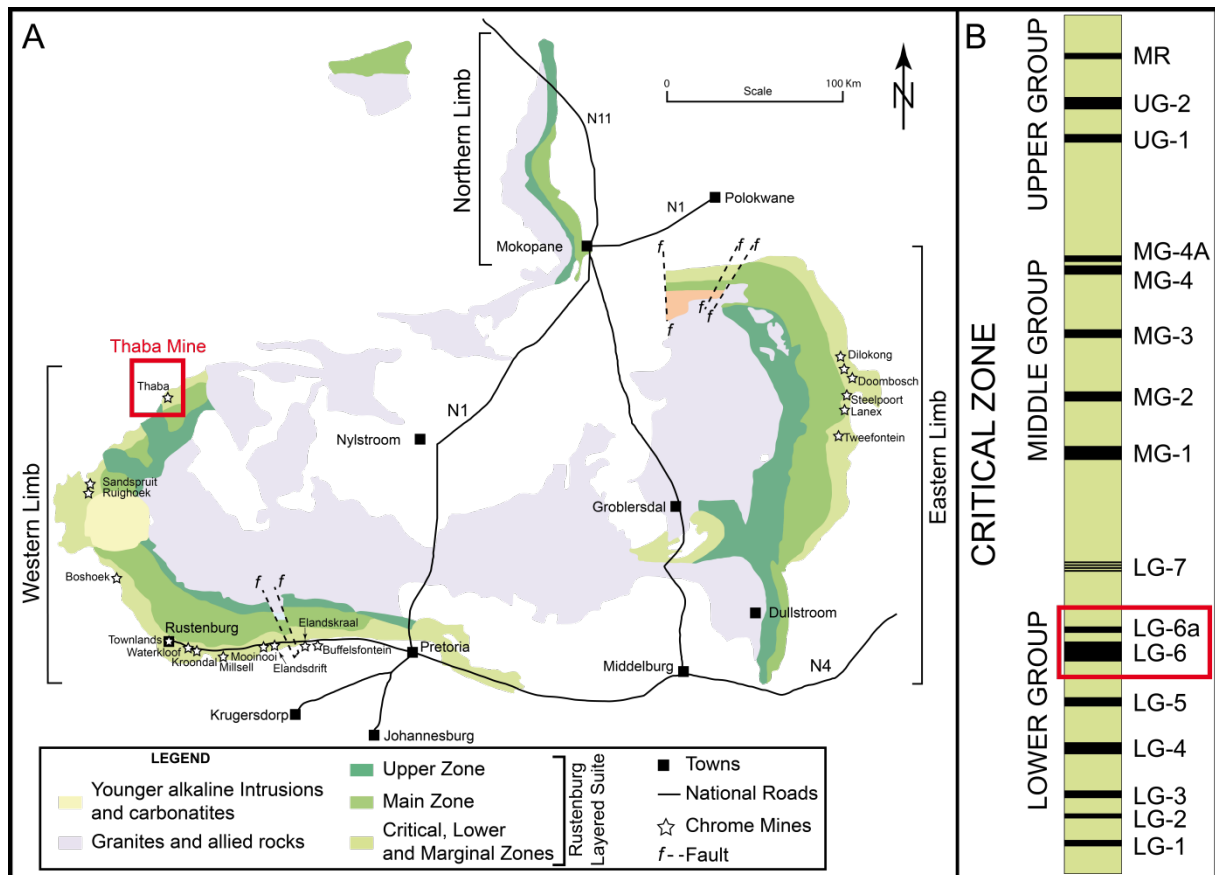
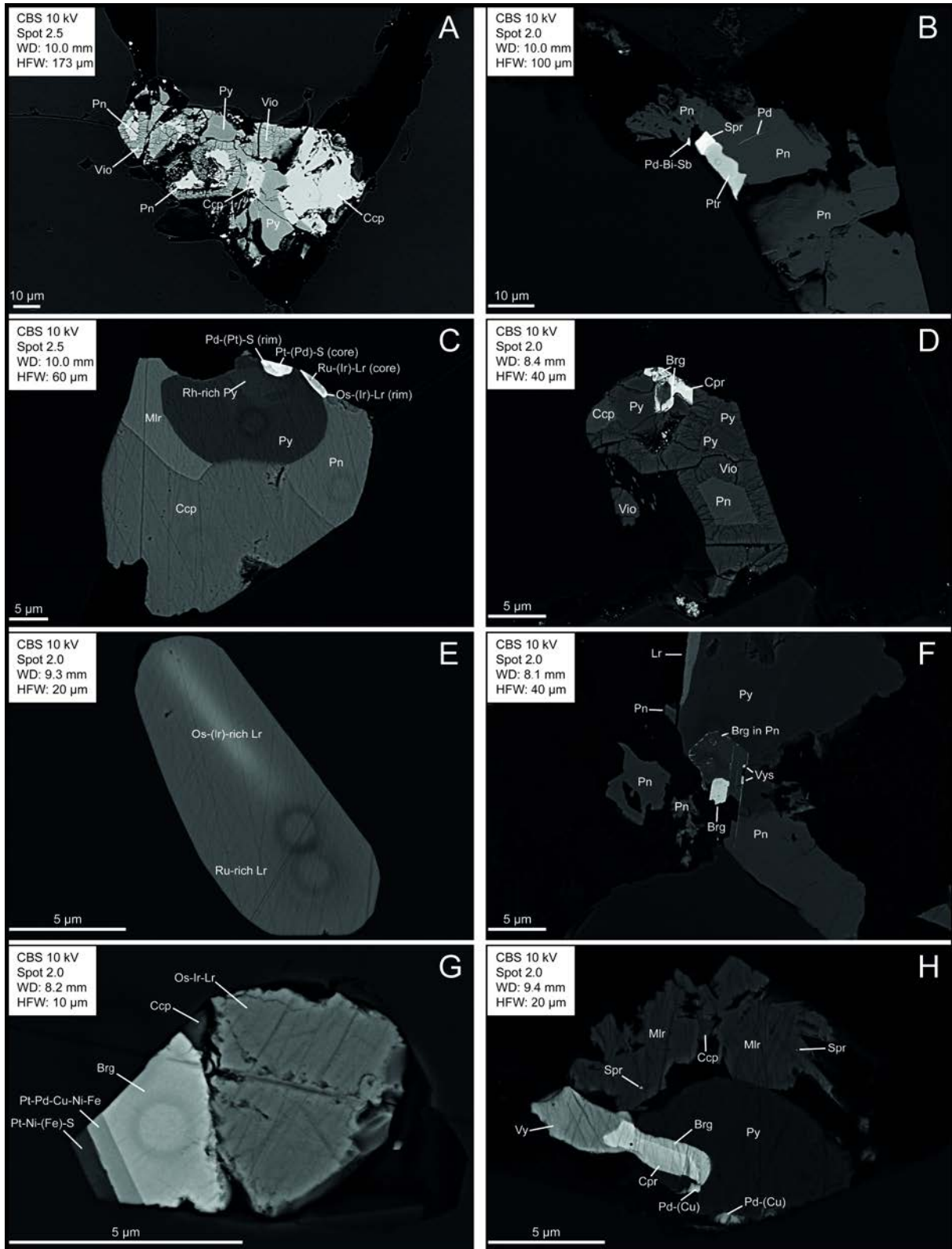
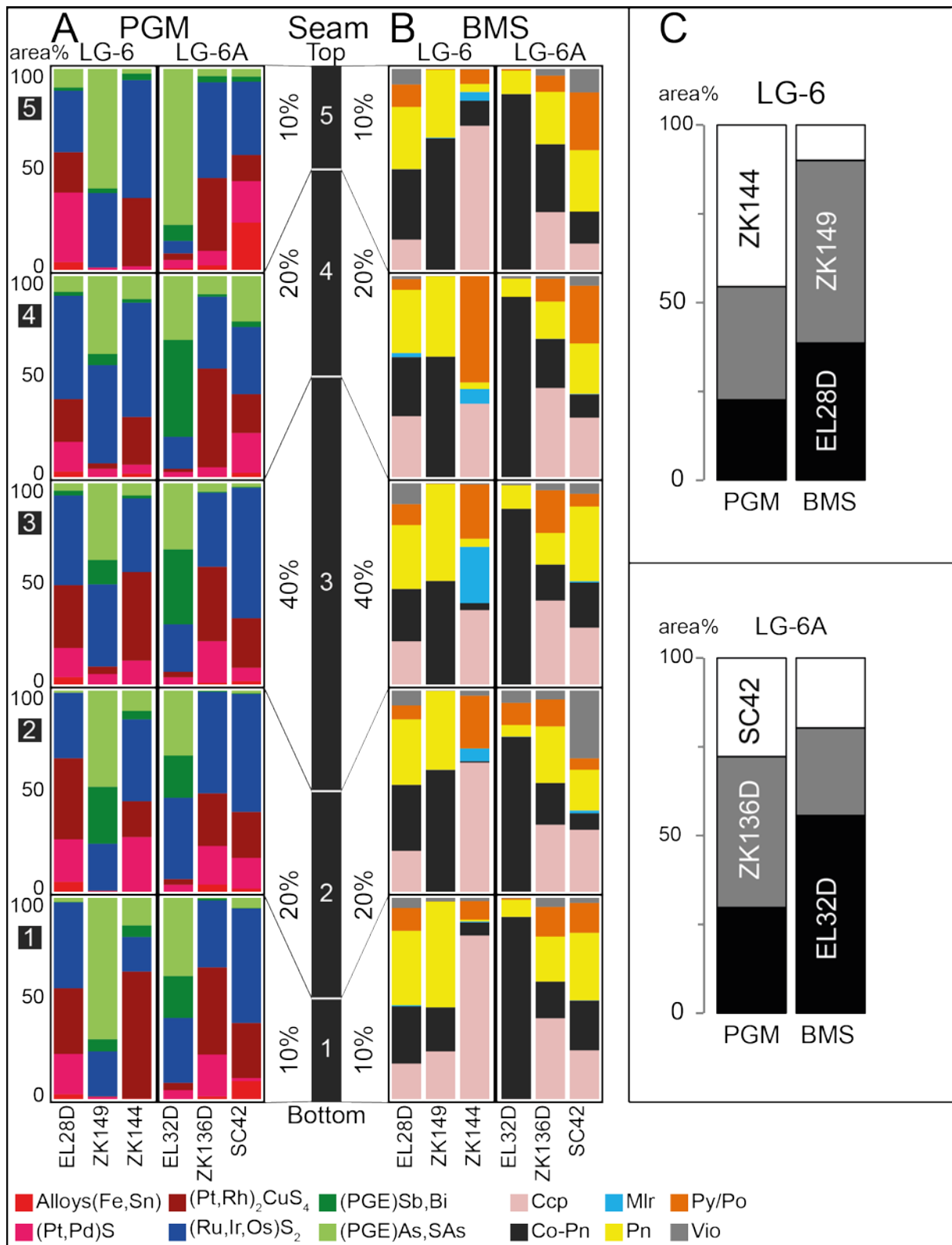


Figure 1(A) Geological map of the Bushveld Complex. The location of the Thaba mine is marked in red. (B) Stratigraphic column of the Critical Zone showing the positions of the major chromitite seams and of the Merensky Reef (MR) (modified from Oberthür et al. 2016).



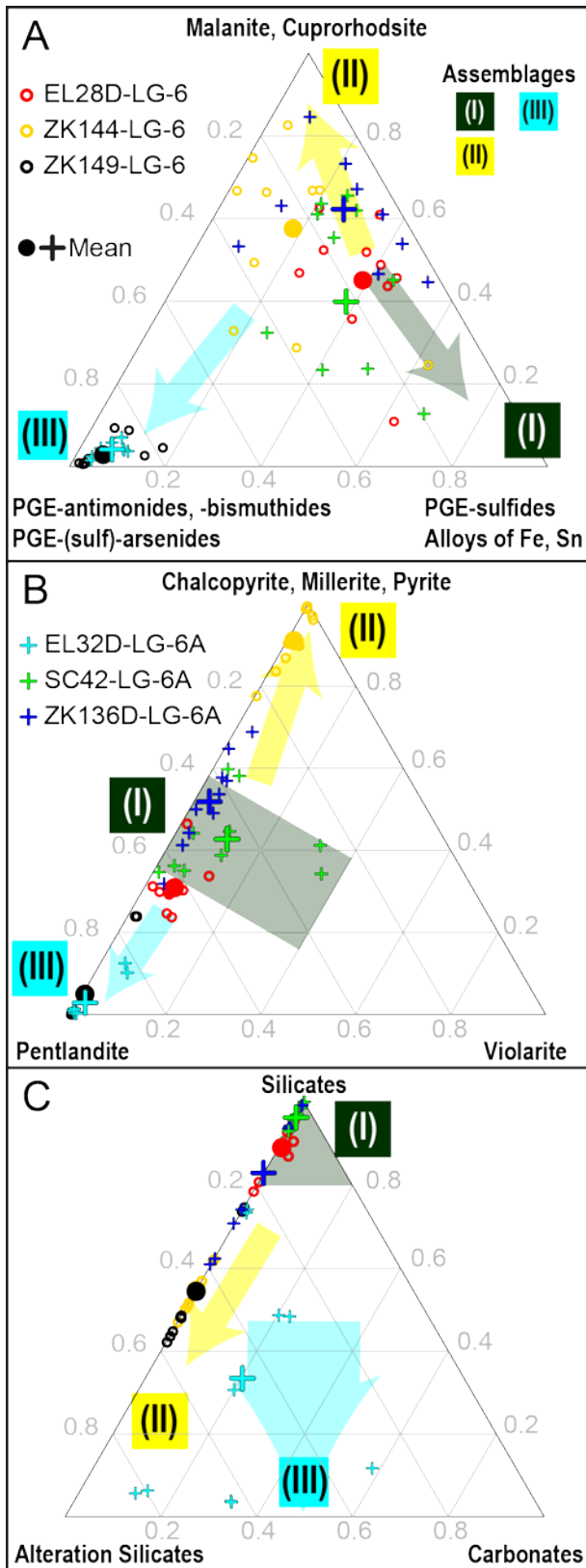
1
 2 Figure 2 Back-scattered electron (BSE) images of sulfides and PGM in polished sections of the LG-6 and LG-6A
 3 chromitite seams. Scale bar and SEM conditions are displayed in the images. (A) Sulfide aggregate containing
 4 pyrite (Py), chalcopyrite (Ccp), pentlandite (Pn) and violarite (Vio) in intersection EL28D-LG-6. Please note the
 5 alteration of pentlandite into violarite. (B) Platarsite (Plr), Sperrylite (Spr) and a PdBiSb alloy intergrown with Pn
 6 in intersection ZK149-LG-6. Please note the Pd dominated lamellae in Pn. (C) Sulfide droplet interstitial to
 7 chromite containing millerite (Mlr), Py, Pn and Ccp in intersection SC42-LG-6A. Note the segregation of PPGE
 8 and IPGE into different discrete PGM (Braggite (Brg) and Laurite (Lr), respectively) as well as the exsolution of
 9 Rh into pyrite (slightly brighter). Both grains show further segregation of Pt and Ru, respectively, located in the
 10 core and Pd and Os in the rim.

11 (Brg) – Cooperite (Cpr) compositions in intersection EL28D-LG-6. Note the alteration of Pn into Vio. (E) Laurite
12 grain as an inclusion in chromite in intersection SC42-LG-6A. Note the brighter area due to a higher
13 concentration of Os and Ir. (F) Brg intergrown with sulfides in intersection ZK136D-LG-6A. Note the exsolution
14 of Pt-Pd into the surrounding sulfides during cooling – keeping the original shape of the Brg grain and the
15 formation of Vysotskite (Vys). (G) PGE particle composed of various PGM, both, sulfides (Brg and Lr) as well as
16 alloys as inclusion in chromite in intersection ZK136D-LG-6A. (H) Pt-Pd sulfide of various composition ranging
17 from Vys to Cpr intergrown with various sulfides in intersection SC42-LG-6A. Note the nanoinclusions of Spr in
18 Mlr and a Pd-Cu rich bright phase.
19

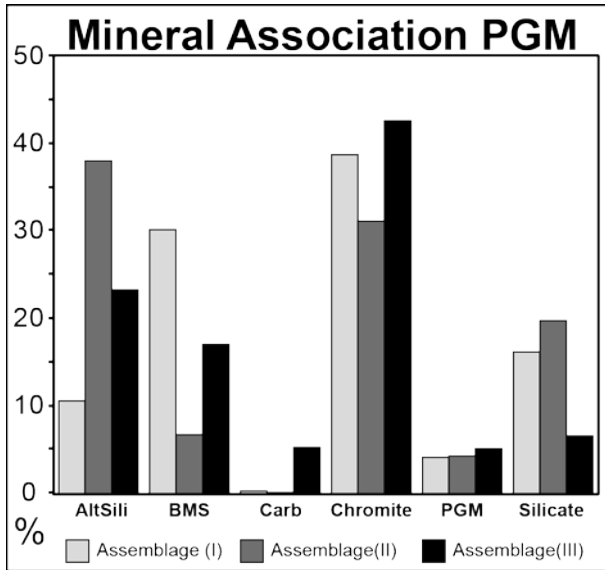


20
21
22
23
24
25
26
27
28
29

Figure 3 Comparison of MLA thin sections data for drill cores of the LG-6 and LG-6A seam intersections. Thirty samples were analyzed for each seam. (A, B) 100% stacked histograms that show the PGM (for detailed grouping see text) (A) and sulfide (B) assemblages of LG-6 and LG-6A intersections from bottom to top (sectors 1 to 5). (C) Based on normalized thin sections, PGM and BMS area within the sample (μm^2) were summed for each drill core separately. The relative distribution of PGM and BMS (area%) in seam LG-6 and LG-6A, respectively, is shown in stacked bar plots. "Seam" displays the division into five sampled distinct sectors (sectors 1-5, from bottom to top) and each sector was sampled randomly to prepare an individual polished thin section for study. For details see text.



30
 31 Figure 4 Modal proportions of all thin sections (and the corresponding means) of LG-6 and LG-6A samples for
 32 (A) PGM, (B) BMS, and (C) Gangue mineral groups projected in a ternary diagram.
 33



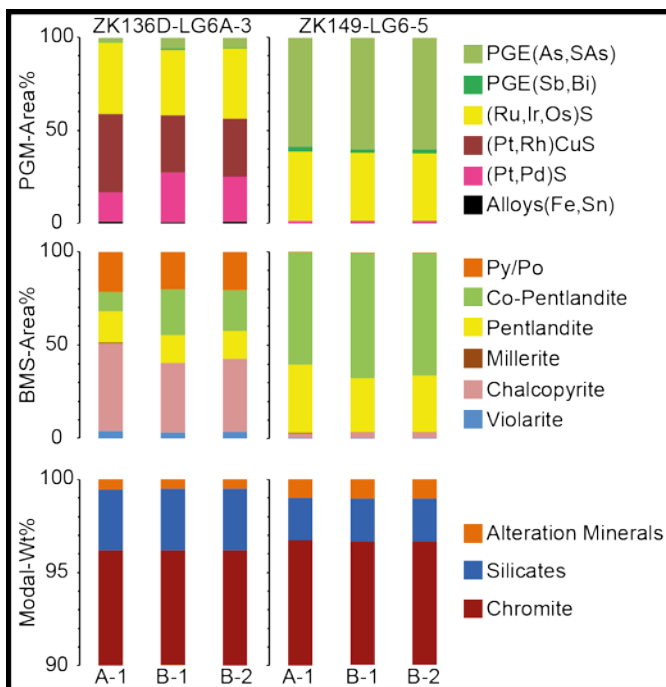
34
 35 Figure 5 Histogram of mineral association of PGM comparing assemblages (I), (II), (III). Assemblage (I) displays
 36 high abundances of PGM-sulfides and alloys of Fe and Sn, while assemblage (II) is dominated by PGM-Cu-
 37 sulfides. Assemblage (III), on the other hand, comprises high amounts of PGM-sulfarsenides and PGM-
 38 arsenides together with PGE-antimonides, -bismuthides and scant -bismuthotellurides.
 39

40

41 **Appendix A**

42 *Methods – Reproducibility of MLA data*

43 Quantification of the reproducibility and statistical significance of the analyses was performed
 44 through (1) analyzing a thin section twice in the same analytical run (in-run duplication), and (2) by
 45 re-polishing of the sample to analyze a second surface of the same sample. Results are displayed in
 46 Figure A1. In-run analysis displays a relative standard deviation (2σ) for total area%^{PGM} of 5 % for
 47 sample ZK149-LG-6 and 4 % for sample ZK136D-LG-6A, while total area%^{BMS} and wt%^{Modal} show 2σ
 48 values below 2 % and 0.5 % for both samples, respectively. The combined in-run duplicates of surface
 49 A with surface B, 2SDs are 32 % in sample ZK149 and 15 % in sample ZK136D-LG-6A for total
 50 area%^{PGM}, while total area%^{BMS} and total area%^{Gangue} show 2σ values below 2 % and 3 % for both
 51 samples, respectively.



52 Figure A1 Stacked histograms showing the proportions of PGM species (in terms of area%^{PGM}), base
 53 metal sulfides (in terms of area%^{BMS}), and the modal mineralogy in wt% for samples ZK136D-LG-6A-3
 54 and ZK149-LG-6-5. A-1: surface A; B-1: surface B-1; B-2: in-run duplicate of surface B-1.
 55

56

57

58 *Methods - Electron probe microanalysis (EPMA)*

59 Quantitative analyses were also performed for amphibole, chromite, clinopyroxene, feldspar, olivine,
60 orthopyroxene, serpentine and talc. Concentrations of Na, Mg, Al (all TAP); Si, K, Ca (all PETJ); Cr, V, Ti
61 (all PETL); Zn, Ni, Co, Fe, Mn (all LIFH) were measured using K_{α} – lines. Certified reference materials
62 provided by ASTIMEX Standards Ltd. were used for calibration. An electron beam diameter of 5 μm
63 was set at 20kV/ 12 nA and the ZAF approach was used for matrix correction (atomic number–
64 absorption–fluorescence; Philibert, 1963; Reed, 1965; Philibert & Tixier, 1968). Dwell times were set
65 to 15s (Na), 20s (Si, Cr, Ni), and 30s (K, Ca, Fe, Mn), 40s (Mg, Al, V, Ti, Zn, Co). Offline overlap
66 corrections were performed for Zn $L_{\beta 1}$ on Na $K_{\alpha 1,2}$; Mn $K_{\alpha 1}$, Ti $K_{\alpha 1}$, Cr $K_{\beta 1,3}$ on Al $K_{\alpha 1,2}$; Ni $K_{\alpha 1}$ on Ca $K_{\alpha 1}$; V
67 $K_{\beta 1,3}$ on Cr $K_{\alpha 1}$; Ti $K_{\beta 1,3}$ on V $K_{\alpha 1}$; Mn $K_{\beta 1,3}$ on Fe $K_{\alpha 1}$; and Cr $K_{\beta 1,3}$ on Mn $K_{\alpha 1}$ as explained in Osbahr et al.
68 (2015).

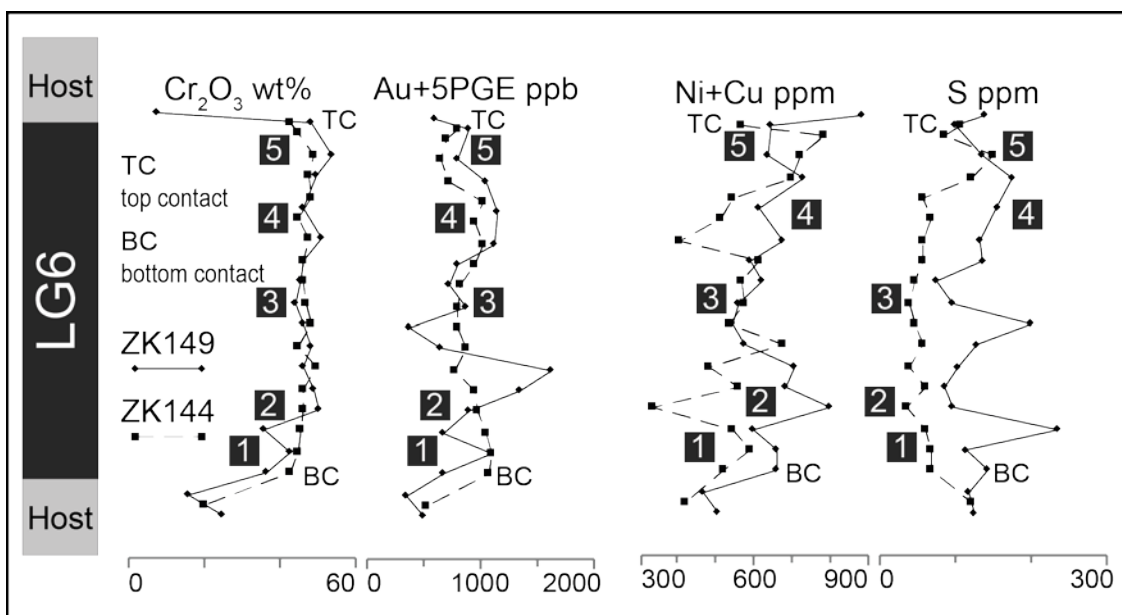
69 Finally, EPMA results were used to generate mineral standard spectra with a known composition for
70 MLA measurements. Therefore, mineral standards were taken close to EPMA measurements. This
71 approach allows a detailed differentiation of silicates, such as different feldspar compositions,
72 amphiboles, pyroxenes and alteration silicates.

73 *Results - Geochemistry*

74 5PGE+Au (Pt,Pd,Rh,Ir,Ru,Au) contents are around 1 ppm for LG-6 samples and 1.5 ppm for the LG-6A.
75 In general, the total sulfur content ranges between 100 – 200 ppm (<250 ppm), except intersection
76 ZK144-LG-6, which contains only around 70 ppm. Detailed information are provided with the
77 electronic supplementary material.

78 Figure A2 displays detailed geochemical assays of two selected drill core intersections of the LG-6
79 (ZK149-LG-6 and ZK144-LG-6). The profiles display a rather stable Cr_2O_3 content around 43-51 wt%.
80 Slight fluctuations, especially in ZK149-LG-6 display massive chromitite intercalated with ~ 1 cm
81 pyroxene-rich bands or pyroxene oikocrysts. 5PGE+Au contents are 900 ppb and 950 ppb with a
82 Pt/Pd ratio around 2.2 and 4 and Pt/Ru ratios around 0.9 for intersections ZK144-LG-6 and ZK149-LG-

83 6, respectively. Both profiles display 5PGE+Au profiles with a “M-shape”; ZK144-LG-6 displays a
 84 smooth variation in the overall PGE contents, ranging from ~700 ppb to 1100 ppb, while ZK149-LG-6
 85 displays spikes with minimum single element contents of roughly 370 ppb and a maximum of
 86 1600 ppb. The Ni+Cu plot displays different patterns, however, with variable contents for both of the
 87 examples. Cu/ (Cu+Ni) ratios are 0.02 and 0.01 for ZK144-LG-6 and ZK149, respectively. In general,
 88 the LG-6 is sulfur poor, with contents ranging from 70 ppm (ZK144-LG-6) to 130 ppm (ZK149-LG-6),
 89 on average.



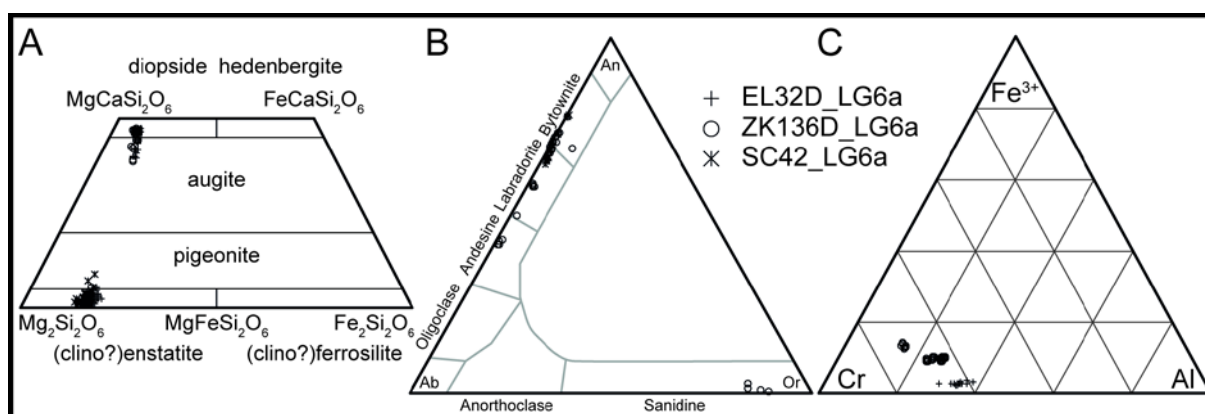
90
 91 Figure A2 Detailed geochemistry of Cr₂O₃, Au+PGE (6E), Ni+Cu, and S concentrations versus
 92 stratigraphic height, normalized to 100 (ZK149: 83 cm; ZK144: 93 cm) in the LG6. Note the bottom
 93 (BC) and top contact (TC) of the intersections. 6E analyzed by Ni fire assay, aqua-regia digestion and
 94 ICP-MS finish, sulfur analyzed by “LECO” combustion.

95 *Results - EPMA analyses – silicate minerals and chromite*

96 Altogether, 359 analyses on LG-6A samples were obtained to describe the mineral chemistry of
 97 various silicate minerals as well as chromite in the LG seams. Table A1 displays representative
 98 analyses of this sample set, extended by some analyses of important mineral compositions, namely
 99 Al-rich chromite, olivine, and serpentine, contained in a MG sample set due to a lack of these
 100 minerals in the measured LG sections. Mineral standard spectra for further MLA analysis were taken
 101 on grains with a known composition for a better identification during quantitative mineralogical
 102 assessment.

103 Figure A3A displays two different types of pyroxenes. One type yields an orthopyroxene $X_{En}=78-85$,
 104 $X_{Fs} = 13-19$ and $X_{Wo} = 0.5-9$ and is hereafter referred to as enstatite. The second type shows a slight
 105 trend from augitic to mainly diopsidic compositions and is composed of $X_{En}=45-52$, $X_{Fs} = 5-9$ and $X_{Wo} =$
 106 $38-48$ (hereafter referred to as diopside). Amphiboles can be best described as magnesio-
 107 hornblende. Feldspars shown in Figure A3B yield plagioclase compositions ranging from andesine to
 108 bytownite, however, also minor albite and anorthite were analyzed by EDX measurement.
 109 Furthermore, sanidine with X_{Or} up to 90 % was encountered. For both, pyroxene and feldspar, there
 110 were no significant differences between samples detected. Chromite was analyzed in sample
 111 EL32D_LG-6A and ZK136D_LG-6A (Figure A3C). Data might indicate differences between samples, as
 112 sample EL32D_LG-6A displays low Fe^{3+} and slightly higher Al contents than ZK136D_LG-6A.

113



114 Figure A3 Ternary plots of EPMA measurements. (A) Classification diagram of pyroxene after
 115 Morimoto (1988). Both types of pyroxene – enstatite (orthopyroxene) and (augite)-diopside are
 116 rather chemically homogeneous. (B) Classification diagram of feldspar with endmembers anorthite
 117 (An), albite (Ab), alkali feldspar/ orthoclase (Or). Beside plagioclase with variable composition alkali
 118 feldspar with sanidine composition was detected. (C) Ternary plot of trivalent cations, Cr, Al and Fe^{3+}
 119 in chromite. Note that the data show only little variation, however, all analyses of intersection
 120 EL32D_LG-6A display a lower concentration in Fe^{3+} compensated by a higher Al content.

122

123

124

125

126

127 Table A1 Representative EPMA analyses of all relevant silicate minerals and chromite, used for the
 128 MLA Mineral Reference List.

No.	346	330	23	207	221	120	228	391	197	445	192	166	132
Core	ZK136D	EL32	EL32D	EL32D	SC42	ZK146	SC42	ZK136D	EL32D	EL32	EL32D	EL32D	ZK146
Seam	LG-6A	MG1	LG-6A	LG-6A	LG-6A	MG1	LG-6A	LG-6A	LG-6A	MG1	LG-6A	LG-6A	MG1
Mineral	Chromite	Al-Chromite	Chromite	ClinoPx	OrthoPx	Olivine	Plagioclase	K-Feldspar	Muscovite	Biotite	Amphibole	Talc	Serpentine
<i>all data in wt%</i>													
Na ₂ O	bdl	bdl	bdl	0.35	0.01	0.02	2.36	1.19	0.11	0.26	1.84	0.05	0.02
MgO	4.84	14.26	6.56	18.00	31.44	45.36	0.04	0.01	0.54	18.84	16.64	25.69	35.97
Al ₂ O ₃	7.43	48.11	17.40	2.00	1.38	0.00	32.54	18.33	34.88	20.71	10.25	0.38	0.01
SiO ₂	0.04	0.72	0.03	53.28	55.32	40.03	49.18	63.29	47.30	39.39	47.60	59.28	40.58
K ₂ O	bdl	bdl	bdl	bdl	0.01	0.00	0.04	15.44	9.66	9.24	0.15	0.02	0.03
CaO	bdl	bdl	bdl	19.44	0.74	0.03	15.64	0.10	0.26	1.52	11.70	0.20	0.03
Cr ₂ O ₃	50.81	14.86	46.53	0.99	0.56	0.00	0.23	bdl	0.02	0.06	2.01	0.09	0.01
V ₂ O ₃	0.46	0.34	0.44	0.05	0.03	0.00	0.01	0.02	0.02	0.01	0.11	0.01	0.01
TiO ₂	0.47	0.05	0.84	0.22	0.09	0.00	bdl	0.04	bdl	0.27	1.30	0.02	0.02
ZnO	0.13	0.76	0.11	bdl	bdl	bdl	bdl	bdl	bdl	bdl	bdl	bdl	bdl
NiO	0.12	0.13	0.14	0.04	0.08	0.29	bdl	0.04	bdl	0.11	0.12	0.05	0.32
CoO	0.13	0.13	0.09	0.02	0.03	0.03	bdl	bdl	0.01	0.02	0.02	0.01	0.03
MnO	0.32	0.09	0.30	0.16	0.24	0.20	bdl	bdl	0.01	0.02	0.08	0.04	0.05
FeO	25.33	16.88	24.52	5.40	9.88	13.92	0.28	0.35	2.24	4.82	5.91	8.69	7.59
Fe ₂ O ₃	9.35	1.60	1.87										
Total	99.42	97.92	98.82	99.97	99.82	99.89	100.31	98.81	95.05	95.27	97.72	94.54	84.68
<i>all data is given as apfu</i>													
Na				0.025	0.001	0.001	0.208	0.108	0.015	0.035	0.198	0.014	
Na (A)											0.315		
Mg	2.019	4.763	2.591	0.979	1.653	1.693	0.003	0.001	0.053	1.981	3.565	5.096	5.302
Al	3.678	19.052	8.152	0.086	0.058		1.748	1.014	2.731	1.722	1.735	0.060	0.002
Al IV				0.055	0.049				0.857	1.221	1.160	0.060	
Al VI				0.031	0.008				1.874	0.502	0.576		0.002
Si	0.024	0.323	0.014	1.945	1.951	1.002	2.241	2.969	3.143	2.779	6.840	7.889	4.012
Si (T1)											2.840		
K							0.003	0.924	0.819	0.831	0.027	0.004	0.004
Ca				0.760	0.028	0.001	0.763	0.005	0.018	0.115	1.802	0.028	0.004
Cr	16.873	3.948	14.627	0.029	0.016		0.008	0.000	0.001	0.004	0.229	0.010	0.001
V	0.160	0.095	0.146	0.002	0.001			0.001	0.001	0.001	0.014	0.001	0.001
Ti	0.199	0.016	0.333	0.006	0.002			0.001		0.014	0.140	0.002	0.001
Zn	0.026	0.126	0.022										
Ni	0.026	0.024	0.029	0.001	0.002	0.006		0.002		0.006	0.014	0.005	0.025
Co	0.029	0.022	0.019	0.001	0.001	0.001			0.001	0.001	0.003	0.001	0.002
Mn	0.076	0.017	0.068	0.005	0.007	0.004			0.001	0.001	0.009	0.004	0.004
Fe ²⁺	5.928	3.163	5.433	0.165	0.291	0.292	0.011	0.014	0.124	0.284	0.710	0.967	0.628
Fe ³⁺	2.955	0.404	0.560										
Vac											0.658		
Total	31.993	31.952	31.995	4.003	4.010	3.000	4.985	5.038	6.907	7.776	15.600	14.082	9.985
Cr/Al	4.587	0.207	1.794										
Mg#	0.254	0.601	0.323	0.86	0.85								
FFE	0.333	0.113	0.093										
Cr#	0.821	0.172	0.642										
Cr/Fe	1.33	0.71	1.56										
Sum IV				2.000	2.000								
Sum VI				2.003	2.010								
X _{Wo}				39.92	1.43								
X _{En}				51.43	83.81								
X _{Fs}				8.65	14.77								
Fo						85.10							
An							78.35	0.50					
Or							0.26	89.08					
X _{Mg}									0.053	0.637	0.834		
Na+K(A)											0.342		

129 Please note the analyses for Al-chromite, olivine, biotite and serpentine were taken from a different
 130 sample set of MG1 samples from the same locality. Calculation of chromite is normalized to 32 O;
 131 pyroxene is normalized to 6 O; olivine is normalized to 4 O; feldspar is normalized to 8 O; mica is
 132 normalized to 11 O; amphibole is normalized to 23 O; talc is normalized to 22 O; and serpentine is
 133 normalized to 14 O. apfu – atoms per formula unit.

134

135 ANOVA

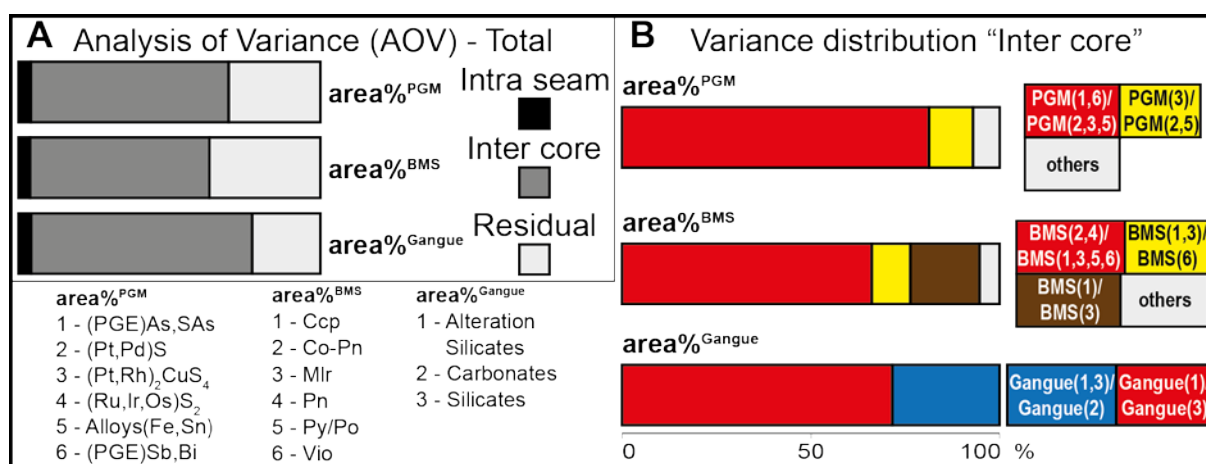
136 An ANOVA was performed – followed by standard F-tests – to investigate the variability of the
137 samples and to determine assemblages for classification according to the sub-compositions
138 $\text{area}\%^{\text{PGM}}$, $\text{area}\%^{\text{BMS}}$ and $\text{area}\%^{\text{Gangue}}$ (see legend in Figure A4A). Variability of the samples was tested
139 for four explanatory factors (“surfaces A/B”, “intra seam”, “inter core” and “inter seam” (see in the
140 methods section for definition of these explanatory factors). “Surfaces A/B” compares the results
141 obtained for the two different polished surfaces (A and B) analysed for each sample. This explanatory
142 factor is found to have no significant influence on the tested ANOVA model, which allows the
143 conclusion that the exact position of the sample surface examined by MLA has no significant effect
144 on the results obtained. Most notably, it suggests that the “nugget effect” (small scale variability) is
145 negligible.

146 The explanatory factor “intra seam” considers the variance between samples of a different
147 stratigraphic position within a sampled seam, *i.e.* if seams have systematically different mineral
148 assemblages within their respective confines. The factor “intra seam” does have a significant
149 influence for the variance of both, $\text{area}\%^{\text{PGM}}$ and $\text{area}\%^{\text{BMS}}$ and a highly significant influence for the
150 variance of $\text{area}\%^{\text{Gangue}}$. The two factors “inter seam” (considering systematic differences between
151 the two studied seams, LG-6 and LG-6A) and “inter core” (considering systematic differences
152 between different drill core intersections) show close interrelation, meaning that variance induced
153 by “inter seam” will be a part of the variance induced by “inter core”. While the F-tests for the factor
154 “inter seam” are non-significant for $\text{area}\%^{\text{PGM}}$ and $\text{area}\%^{\text{BMS}}$, and highly significant for $\text{area}\%^{\text{Gangue}}$, the
155 factor “inter core” yields highly significant results in all cases. This suggests that systematic
156 differences between distinct seams intersected within the same drill core are of minor importance
157 compared to differences encountered between drill cores from different sites on the mine lease
158 area.

159 Figure 4A shows the variance distribution for the two most relevant factors. “Inter core” is by far the
160 most important explanatory factor, explaining between 59 and 77 % of the total variance. In
161 comparison, the factor “intra core” explains only 6 % of total variance – a value that is similar for all
162 sub-compositions. As mentioned above, the factor “seam” was not considered further, as it explains
163 only between 2 and 13 % of the “inter core” variance for $\text{area}\%^{\text{PGM}}$ and $\text{area}\%^{\text{BMS}}$ and $\text{area}\%^{\text{Gangue}}$. The
164 factor “residuals” reports the variance that cannot be assigned to any of the previously mentioned
165 factors and ranges between 23 and 35 % of the total variance. A detailed evaluation of the
166 explanatory factor “inter core” for all sub-compositions based on ratios of certain mineral groups is
167 shown in Figure A4B. The chosen ratios explain the bulk total variance, *i.e.* reflect the distribution of
168 the group members. According to the ANOVA model the main part of the total variance in $\text{area}\%^{\text{PGM}}$
169 is invested in predicting the ratios [PGE -sulfarsenides and PGE-antimonides, -bismuthides vs. PGE –
170 sulfides, -Cu-sulfides and -alloys of Fe,Sn]; *i.e.* these groups show a strong negative correlation and
171 form distinctly different mineral assemblages. Furthermore, the ratio [PGE-Cu-sulfides vs. PGE –
172 sulfides and –alloys of Fe,Sn] explains a significant portion of the total variance, and may be used to
173 distinguish two more PGM mineral assemblages. The variability of IPGE -sulfides is rather low and
174 only marginally explained by the factor “inter core”. The $\text{area}\%^{\text{BMS}}$ “inter core” variance is mostly
175 related to the variability of (Co-rich) pentlandite with respect to the geometric average of the other
176 four BMS considered (chalcopyrite, millerite, pyrite and violarite). The ratios [chalcopyrite vs.
177 millerite] and [chalcopyrite and millerite vs. violarite] do also have relevant contributions. The
178 mentioned relationships correspond well to the $\text{area}\%^{\text{PGM}}$ distribution, *i.e.* PGE-sulfarsenide/ -alloy of
179 Sb,Bi-rich assemblages represent the same set of samples as the (Co-rich) pentlandite dominated
180 BMS assemblages (forming assemblage (III)). On the other hand, PGE-(Cu)–sulfides and -alloys of
181 Fe,Sn occur together with rather chalcopyrite, millerite, pyrite, violarite dominated samples –
182 resulting in assemblage (I) and (II). The latter assemblages can be further subdivided into PGE-Cu-
183 sulfides + chalcopyrite and millerite-rich samples (assemblage (II)), in contrast to assemblage (I)

184 where a PGE-sulfide-rich assemblage is associated with a rather variable BMS assemblage consisting
 185 of chalcopyrite, pentlandite, pyrite and variable amounts of violarite.

186 In the $area\%^{Gangue}$ sub-composition total “inter core” variance is best described using the ratios
 187 [alteration silicates and silicates vs. carbonate] followed by [alteration silicates vs. silicates]. While
 188 carbonate-rich samples are associated with PGM-BMS assemblage (III), silicate-rich samples
 189 dominate PGM-BMS assemblage (I). Significant amounts of alteration silicates may occur in samples
 190 belonging to PGM-BMS assemblages (II) and (III).



191 Figure A4 Stacked histograms of the results of an analysis of variance (AOV) of the modal mineralogy
 192 for PGM, BMS and rock forming minerals (Others). (A) Total variance distribution for $area\%^{PGM}$,
 193 $area\%^{BMS}$ and $area\%^{Gangue}$. (B) Variance distribution based on defined ratios of certain
 194 PGM/BMS/Gangue groups. For simplification, further reference to any group members will be as
 195 following, e.g. (PGE)As,AsS = PGM(1); Alloys(Sb,Bi) = PGM(6); Ccp = BMS(1), etc. (cf. Table 6; legend
 196 in (A)).
 197
 198

199 Cluster analysis

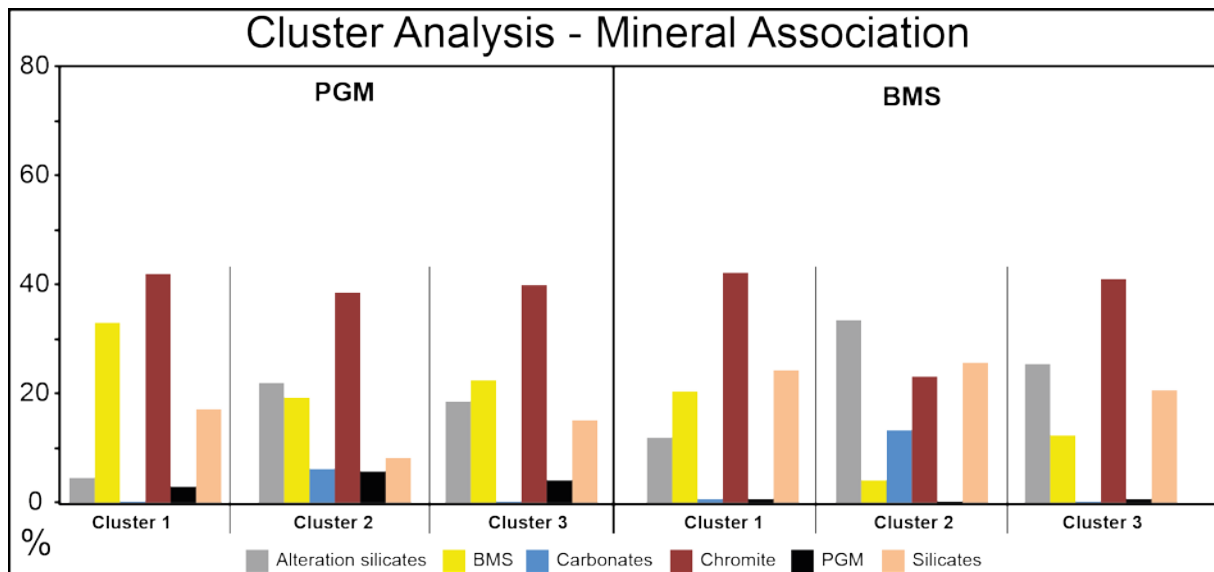
200 For a quantitative assessment of the variability of the mineral association a cluster analysis was
 201 performed according to the sub-compositions of PGM (without IPGE sulfides) and BMS. The results
 202 were linked to the mineral assemblages defined in the previous chapter (ANOVA).

203 Despite the very low total abundance of BMS (< 0.02 area% in all samples), PGM show a strong
 204 preferred association with BMS; they also show a close association with alteration silicates, occurring
 205 both in interstitial positions and as inclusion. PGM are only to a much lesser extent associated with

206 silicates and chromite. PGM occur predominantly interstitial to chromite (with minor inclusions cf.
207 Figure 2G). BMS show a very similar association to PGM.

208 The cluster analysis results in three distinct clusters: a dominant and two minor, for both PGM
209 [$n_{\text{Cluster1}} = 5$, $n_{\text{Cluster2}} = 16$, $n_{\text{Cluster3}} = 39$] and for BMS [$n_{\text{Cluster1}} = 39$, $n_{\text{Cluster2}} = 12$, $n_{\text{Cluster3}} = 9$] (Figure A5).

210 PGM cluster 1 consists of samples with a high silicate and lower chromite content, where most PGM
211 occur in association with BMS. Cluster 2 includes carbonate-rich samples and PGM associated with
212 alteration silicates and carbonates. Cluster 3, on the other hand, represents high chromite, high
213 alteration silicate and low silicate content samples; PGM in this cluster are intergrown with alteration
214 silicates and silicates. BMS cluster 1 is marked by high silicate/ alteration silicate ratios, where BMS
215 occur predominantly as polymineralic aggregates intergrown with both alteration silicates and
216 silicates. In contrast, the BMS cluster 3 lacks BMS aggregates and includes samples with low
217 silicate/alteration silicate ratios. BMS are closely associated with silicates and alteration silicates in
218 these samples. Similar to PGM cluster 2, the BMS cluster 2 represents carbonate-rich samples. Both,
219 PGM and BMS mineral associations thus define similar clusters - implying a separation of silicate-
220 dominated from alteration silicate and/or carbonate-dominated clusters. BMS and PGM tend to be
221 associated with alteration minerals, if present, hence, establishing cluster 1 as typical for assemblage
222 (I) seems valid. Furthermore, cluster 2 can be assigned to assemblage (III), while cluster 3 mainly
223 represents the alteration silicate-rich members of assemblage (II) and (III).



224 Figure A5 Histograms of average mineral associations of clusters defined by two cluster analysis for
 225 sub-compositions PGM (without IPGE –sulfides) and BMS, respectively. Color codes are explained
 226 below corresponding histograms. Cluster (I) displays high abundances of PGM-sulfides and alloys of
 227 Fe and Sn together with BMS dominated by pentlandite + chalcopyrite + pyrite. Cluster (II) comprises
 228 high amounts of PGM-sulfarsenides and PGM-arsenides together with PGE-antimonides, -
 229 bismuthides and scant –bismuthotellurides. Corresponding BMS are strongly dominated by
 230 pentlandite and Co-rich pentlandite. On the one hand, cluster (III) represents samples dominated by
 231 PGM-Cu-sulfide corresponding with high amounts of chalcopyrite. On the other hand, a minor
 232 amount of samples contains significant portions of PGM-sulfarsenides, -arsenides, -antimonides, and
 233 -bismuthides corresponding with a high abundance of pentlandite.
 234
 235

236 *References*

237 Morimoto N (1988) Nomenclature of pyroxenes. *Mineralogy and Petrology* 39(1):55–76

238 Philibert J (1963) X-ray optics and x-ray microanalysis. In *Proceedings of the Third International*
 239 *Symposium, Stanford University, Pattee H.H., Cosslett, V.E. & Engström, A. (Eds.), New York,*
 240 *NY: Academic Press: 379*

241 Philibert J, Tixier R (1968) Electron penetration and the atomic number correction in electron probe
 242 *microanalysis. J Phys 1: 685–694*

243 Reed SJB (1965) Characteristic fluorescence corrections in electron probe microanalysis. *Br J Appl*
 244 *Phys 16: 913–926*